Contents lists available at ScienceDirect

Earth-Science Reviews

journal homepage: www.elsevier.com

Infragravity waves: From driving mechanisms to impacts

Xavier Bertin[a, *], Anouk de Bakker[a], Ap van Dongeren[c], Giovanni Coco[d], Gael André[e], Fabrice Ardhuin[f], Philippe Bonneton[g], Frédéric Bouchette[h], Bruno Castelle[g], Wayne C. Crawford[i], Mark Davidson[p], Martha Deen[i], Guillaume Dodet[b], Thomas Guerin[a], Kris Inch[p], Fabien Leckler[e], Robert McCall[c], Héloïse Muller[j], Maitane Olabarrieta[k], Dano Roelvink[l], Gerben Ruessink[m], Damien Sous[n], Éléonore Stutzmann[i], Marion Tissier[o]

[a] UMR 7266 LIENSs CNRS-Université de La Rochelle, Institut du Littoral et de l'Environnement, 2 rue Olympe de Gouges, La Rochelle 17000, France
[b] Université de Bretagne Occidentale, CNRS, UMR LETG 6554 GEOMER, IUEM, Technopôle Brest-Iroise, Plouzané 29280, France
[c] Department ZKS, Deltares, PO Box 177, Delft 2600MH, The Netherlands
[d] School of Environment, University of Auckland, New Zealand
[e] SHOM, 13 Rue de Chatellier, Brest 29200, France
[f] Laboratoire d'Océanographie Physique et Spatiale, Univ. Brest/CNRS/Ifremer/IRD, Plouzané 29200, France
[g] UMR EPOC, University of Bordeaux/CNRS, Bordeaux, France
[h] UMR GEOSCIENCES-Montpellier, CNRS/Université de Montpellier II, Montpellier, France
[i] Institut de Physique du Globe de Paris, PRES Sorbonne Paris Cité, CNRS UMR 7154, 1 rue Jussieu, Paris 75005, France
[j] Risks and Prevention Direction, BRGM, 3, avenue Claude Guillemin, Orléans 45060, France
[k] Civil and Coastal Engineering Department, ESSIE, University of Florida, Gainesville, Florida, USA
[l] IHE, Delft, The Netherlands
[m] Department of Physical Geography, Faculty of Geosciences, Utrecht University, Utrecht, The Netherlands
[n] Université de Toulon, Aix Marseille Université, CNRS, IRD, Mediterranean Institute of Oceanography (MIO), La Garde, France
[o] Environmental Fluid Mechanics Section, Faculty of Civil Engineering and Geosciences, Delft University of Technology, Stevinweg 1, Delft 2628CN, The Netherlands
[p] School of Biological and Marine Sciences, Plymouth University, Drake Circus, Plymouth PL4 8AA, United Kingdom

ARTICLE INFO

Keywords:
Infragravity waves
Bound wave
Dissipation
Reflection
Sediment transport
Barrier breaching
Seiche
Earth hum

ABSTRACT

Infragravity (hereafter IG) waves are surface ocean waves with frequencies below those of wind-generated "short waves" (typically below 0.04 Hz). Here we focus on the most common type of IG waves, those induced by the presence of groups in incident short waves. Three related mechanisms explain their generation: (1) the development, shoaling and release of waves bound to the short-wave group envelopes (2) the modulation by these envelopes of the location where short waves break, and (3) the merging of bores (breaking wave front, resembling to a hydraulic jump) inside the surfzone. When reaching shallow water (O(1–10 m)), IG waves can transfer part of their energy back to higher frequencies, a process which is highly dependent on beach slope. On gently sloping beaches, IG waves can dissipate a substantial amount of energy through depth-limited breaking. When the bottom is very rough, such as in coral reef environments, a substantial amount of energy can be dissipated through bottom friction. IG wave energy that is not dissipated is reflected seaward, predominantly for the lowest IG frequencies and on steep bottom slopes. This reflection of the lowest IG frequencies can result in the development of standing (also known as stationary) waves. Reflected IG waves can be refractively trapped so that quasi-periodic along-shore patterns, also referred to as edge waves, can develop. IG waves have a large range of implications in the hydro-sedimentary dynamics of coastal zones. For example, they can modulate current velocities in rip channels and strongly influence cross-shore and longshore mixing. On sandy beaches, IG waves can strongly impact the water table and associated groundwater flows. On gently sloping beaches and especially under storm conditions, IG waves can dominate cross-shore sediment transport, generally promoting

* Corresponding author.
Email addresses: xbertin@univ-lr.fr (X. Bertin); anouk.de_bakker@univ-lr.fr (A.d. Bakker); Ap.vanDongeren@deltares.nl (A.v. Dongeren); g.coco@auckland.ac.nz (G. Coco); gael.andre@shom.fr (G. André); ardhuin@ifremer.fr (F. Ardhuin); p.bonneton@epoc.u-bordeaux1.fr (P. Bonneton); frederic.bouchette@gm.univ-montp2.fr (F. Bouchette); b.castelle@epoc.u-bordeaux1.fr (B. Castelle); crawford@ipgp.fr (W.C. Crawford); M.Davidson@plymouth.ac.uk (M. Davidson); deen@ipgp.fr (M. Deen); guillaume.dodet@univ-brest.fr (G. Dodet); thomas.guerin@univ-lr.fr (T. Guerin); kris.inch@plymouth.ac.uk (K. Inch); fabien.leckler@shom.fr (F. Leckler); Robert.McCall@deltares.nl (R. McCall); heloise.muller@gmail.com (H. Muller); maitane.olabarrieta@essie.ufl.edu (M. Olabarrieta); d.roelvink@un-ihe.org (D. Roelvink); B.G.Ruessink@uu.nl (G. Ruessink); damien.sous@mio.osupytheas.fr (D. Sous); stutz@ipgp.fr (É. Stutzmann); m.f.s.tissier@tudelft.nl (M. Tissier)

https://doi.org/10.1016/j.earscirev.2018.01.002
Received 20 June 2017; Received in revised form 22 December 2017; Accepted 3 January 2018
Available online xxx
0012-8252/

offshore transport inside the surfzone. Under storm conditions, IG waves can also induce overwash and eventually promote dune erosion and barrier breaching. In tidal inlets, IG waves can propagate into the back-barrier lagoon during the flood phase and induce large modulations of currents and sediment transport. Their effect appears to be smaller during the ebb phase, due to blocking by countercurrents, particularly in shallow systems. On coral and rocky reefs, IG waves can dominate over short-waves and control the hydro-sedimentary dynamics over the reef flat and in the lagoon. In harbors and semi-enclosed basins, free IG waves can be amplified by resonance and induce large seiches (resonant oscillations). Lastly, free IG waves that are generated in the nearshore can cross oceans and they can also explain the development of the Earth's "hum" (background free oscillations of the solid earth).

1. Introduction

Infragravity (hereafter IG) waves are surface ocean waves with frequencies below those of wind-generated "short waves". Typical short-wave frequencies are between 0.04 and 1 Hz whereas IG wave frequencies are generally defined as being between 0.004 and 0.04 Hz. For a given water depth, IG waves have longer wavelengths than short waves: for example, at a water depth of 10 m, IG waves have wavelengths from a few hundred meters to kilometres whereas short-waves have wavelengths from a few meters to hundreds of meters.

While the first observations of IG waves date back only to the middle of the 20th century (Munk, 1949), it is now well recognized that IG waves contribute considerably to nearshore hydrodynamics (e.g. Guza and Thornton, 1982; Elgar et al., 1992; Reniers et al., 2002; Ruessink et al., 1998a; Pomeroy et al., 2012; Guedes et al., 2013), sediment transport (e.g. Russell, 1993; Aagaard and Greenwood, 2008; De Bakker et al., 2016), dune and barrier breaching (e.g. Roelvink et al., 2009), development of seiche in harbours (e.g. Okihiro et al., 1993) and they are considered to be the source of background free oscillations of the solid earth, also referred to as "the hum of the Earth" (e.g. Webb, 2007; Rhie and Romanowicz, 2006). This large range of implications probably explains the growing interest in IG waves over the last decade, as it is attested by the increasing volume of literature on the topic (Fig. 1).

Munk (1949) was the first to identify a relation between low frequency motions along the shoreline and the presence of groups in the incident short waves. He also found that the amplitude of these long waves was approximately proportional to that of incident short waves but independent of their period. Tucker (1950) performed a cross-correlation between the short wave energy envelope and the IG wave amplitude and confirmed the existence of a linear relation between the two. A few years later, Biesel (1952) provided the first mathematical demonstration of the existence of secondary long waves forced by incident short waves. Applying their concept of radiation stress (the momentum flux associated with the short waves) to a 1D bichromatic wave field, Longuet-Higgins and Stewart (1962) demonstrated that groups in the incident short waves can force a so-called bound wave, 180 ° out of phase with the amplitude of the short-wave group.

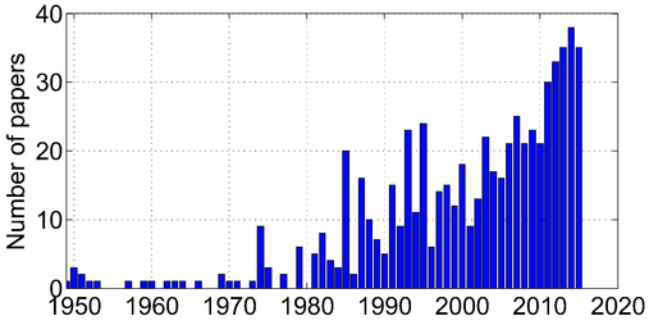

Fig. 1. Number of paper per year found in Scopus and Web of Science where the title includes infragravity waves or surf-beat.

Hasselmann (1962) extended this finding to a 2D random wave field, deriving an analytical solution to compute the bound wave from the directional spectra of the incident short waves. In the 1970s, Gallagher (1971) showed that IG waves reflected at the shoreline can be refractively trapped in the nearshore, so that quasi-stationary along-shore patterns, referred to as edge waves, can develop. This finding was later corroborated by Bowen and Guza (1978) and many others. The so-called pattern theory was developed in the same period and proposes that such edge waves can imprint the morphology and explain the development of periodic 3D patterns on sandy beaches (Bowen and Inman, 1971; Holman and Bowen, 1982). Although this theory was challenged by self-organization theories over the last 15 years (e.g. Falqueś et al., 2000; Coco and Murray, 2008), it fostered much research on IG waves in the period 1970–2000. In that period, Symonds et al. (1982) proposed an additional generation mechanism for IG waves, where the variation of the breakpoint (the location where short waves break) on the timescale of wave groups releases free long waves both shoreward and seaward of the breaking zone. A decade later, Schäffer (1993) combined the two main generation mechanisms of IG waves (i.e. bound wave and varying breakpoint) into one semi-analytical model.

Field experiments in the 80's and 90's provided important new insights into IG-wave dynamics. Following Munk (1949) and Tucker (1950), trends between offshore short-wave height and IG-wave height were identified in the field (e.g. Holman, 1981; Guza and Thornton, 1982; Guza and Thornton, 1985; Huntley et al., 1993). The first method for separating the incoming and outgoing (free) IG-wave signals was developed by Guza et al. (1984), and triggered the study of reflection patterns of IG waves. At the same time, bispectral analysis (Hasselmann et al., 1963) offered a more detailed understanding of the mechanisms responsible for IG-wave generation (e.g. Elgar and Guza, 1985; Herbers et al., 1994; Herbers and Burton, 1997; Norheim et al., 1998; Ruessink, 1998a) which demonstrated, for instance, the importance of directional spreading and the spectral shape of incident short waves on the resulting IG-wave energy. Furthermore, e.g., Guza and Thornton (1982) ; Guza et al. (1984) ; Holman and Sallenger (1985) ; Raubenheimer et al. (1996) ; Ruessink et al. (1998a) ; Ruggiero et al. (2004) established the importance of IG waves in run-up(the maximum vertical extent of wave uprush on a beach), with a particularly large influence on mildly sloping beaches under energetic wave conditions. In addition, many field studies investigated the suspension and cross-shore transport of sand by IG waves (e.g. Abdelrahman and Thornton, 1987; Beach and Sternberg, 1988; Roelvink and Stive, 1989; Shibayama et al., 1991; Osborne and Greenwood, 1992; Russell, 1993). However, contrasting conclusions were reached in terms of transport direction and the respective contribution of IG waves, suggesting that parameters such as the beach profile or incident short-wave conditions are also important.

From the late 90's onwards, laboratory experiments offered a more detailed view of IG waves. The Boers (1996) experiment and, more recently, the GLOBEX experiment (Ruessink et al., 2013), and the subsequent analyses resulted in strong improvements concerning the understanding of generation mechanisms, propagation (such as IG wave

height growth and phase correlation with the short-wave envelope) and dissipation trends and mechanisms (e.g. Janssen et al., 2003; Battjes et al., 2004; Van Dongeren et al., 2007; De Bakker et al., 2015a; Inch et al., 2017a).

Over the last 15 years, the development of numerical models capable of simulating the generation and propagation of IG waves in the nearshore started to emerge, following two distinct approaches. The first approach couples a circulation model with a spectral, phase-averaged, model representing energy fluctuations at the scale of short-wave groups (e.g. Van Dongeren et al., 2003; Reniers et al., 2004; Roelvink et al., 2009). The second approach, known as phase-resolving, explicitly represents the short waves and their induced circulation, including the detailed interactions between short waves and IG waves (e.g. Kennedy et al., 2000; Zijlema et al., 2011; Bonneton et al., 2011; Sheremet et al., 2016).

Over the past decade, many studies have combined numerical modelling with field or laboratory experiments to improve understanding of the processes controlling the generation mechanisms, the propagation and the transformation of IG waves (e.g. De Bakker et al., 2015b; Rijnsdorp et al., 2015; Bertin and Olabarrieta, 2016), as well as their impacts on sediment dynamics and barrier breaching (e.g. Roelvink et al., 2009), and on the hydrodynamic circulation in coral reefs (e.g. Pomeroy et al., 2012, Van Dongeren et al., 2013). In addition, over the past years the importance of IG waves in other environments has been identified, varying from their role in the creation of acoustic wave activity in the thermosphere (Godin et al., 2015; Zabotin et al., 2016), their impact on cliff top shaking (Earlie et al., 2015; Young et al., 2016), to their influence on iceshelf collapse in the Antarctic (e.g. Bromirski et al., 2015).

This paper reviews the state-of-the-art in knowledge about IG waves and gives an overview of the large range of impacts associated with this phenomenon. This initiative follows a workshop that took place in La Rochelle (France) on the 17–18th March 2016 and gathered a substantial part of the European community working on IG waves. Section 2 reviews the main generation mechanisms for IG waves. Section 3 summarizes the main transformations that IG waves experience in the nearshore. The next section presents a large range of effects IG waves have in various coastal environments, spanning from sediment transport to the development of seiches in harbours or the Earth's hum. The last section provides a conclusion and discusses the future challenges concerning research on IG waves.

2. Generation mechanisms

2.1. Bound wave

Biesel (1952), followed by Longuet-Higgins and Stewart (1962), demonstrated that the presence of groups in incident short waves can force a secondary wave of a similar frequency as the group, a so-called bound wave. Bound IG waves are already generated in deep water, and, although they are small (on the order of 1 cm), they undergo a significant transformation and growth in height when propagating from deep water to the shoreline. In a conceptual description, consider two short waves at discrete frequencies (a so-called bichromatic wave field) propagating over a horizontal bed (Fig. 2-A). Since the two waves travel at slightly different celerities, the amplitudes of the waves locally add up or cancel out. This pattern creates wave groups whose frequency is equal to the difference between the frequencies of the two considered short waves (Fig. 2-B). In general, this frequency difference is about one order of magnitude lower than the frequency of the short waves. Through nonlinear (second-order Stokes) interactions, the waves force a slight depression and rise in the mean sea level at the wave group length. This undulation can be seen as a wave itself and it is in anti-phase with the wave groups. In other words, waves with higher amplitudes transport more momentum than small waves, thereby pushing the mean water level down under higher waves and creating a relative water level set-up at the location of the smaller waves (Fig. 2-B). This long wave travels phase-locked to the wave group, and is therefore called a bound wave (Biesel, 1952; Longuet-Higgins and Stewart, 1962). Longuet-Higgins and Stewart (1962) derived an equilibrium solution that relates the bound wave amplitude to

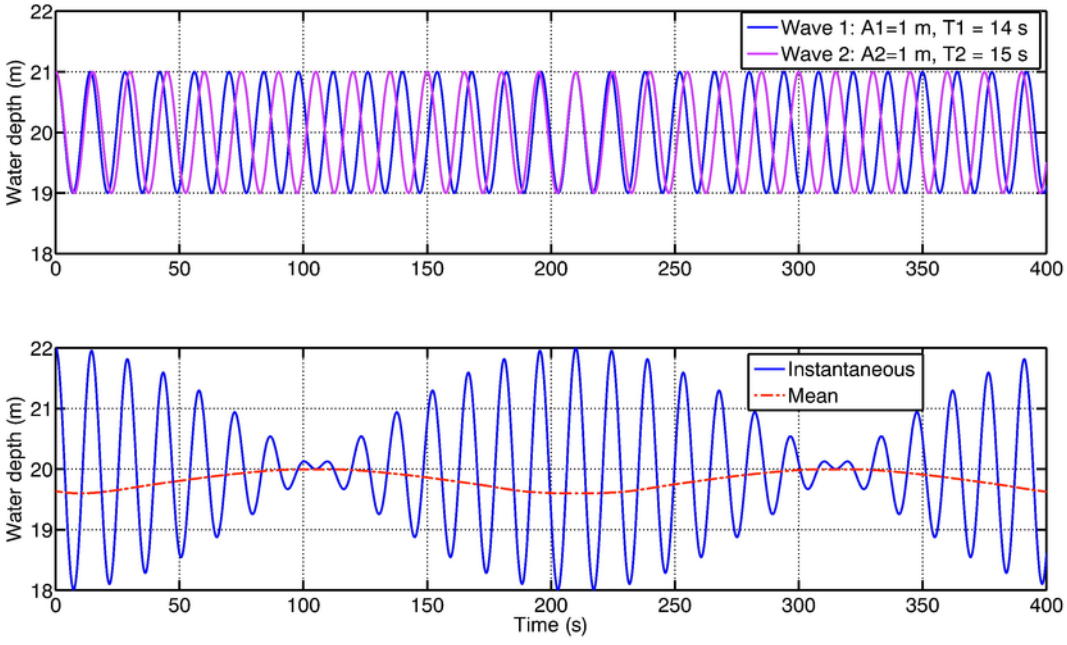

Fig. 2. (A) Time series of two sinusoidal waves with periods of 14 s (blue) and 15 s (pink) travelling over a flat bottom by 20 m water depth. (B) Resulting free surface elevation (blue) and bound wave (red) as computed according to Longuet-Higgins and Stewart (1962).

the energy of the short waves:

$$\eta(x,t) = \frac{-S_{xx}(x,t)}{\rho\left(gh - c_g^2\right)} + K \quad (1)$$

In this equation, S_{xx} is the wave radiation stress, which corresponds to the momentum flux associated with short waves, h is the mean water depth, ρ is the water density, g is the gravitational acceleration, c_g is the short waves group velocity and K is a constant. The theoretical results were validated with observational data in the laboratory (e.g. Kostense, 1984; Baldock et al., 2000).

In nature, the short wave field is composed of a large number of random components and through sub-harmonic interactions, a spectrum of bound wave components is forced according to mechanisms described by Hasselmann (1962) and Herbers et al. (1994), which in effect is a two-dimensional generalization of Longuet-Higgins and Stewart (1962). These bound IG waves typically have frequencies in the range of 0.004 –0.04 Hz, and in deeper water have amplitudes of mere centimetres. However, the equilibrium solution proposed by Longuet-Higgins and Stewart (1962) is only valid for a flat bottom. For a sloping bottom, the bound wave is no longer in equilibrium with the energy envelope of the short waves. As the wave groups propagate into shallower water, the phase difference between the wave groups and the bound wave shifts away from 180 °, so that the long waves lag behind the wave groups. This phenomenon was observed in the field (e.g. Masselink, 1995; Inch et al., 2017a), was reproduced numerically by List (1992), was observed during laboratory experiments by Battjes et al. (2004) and De Bakker et al. (2013) and was explained theoretically by Janssen et al. (2003). This phase shift allows energy transfer from short waves to the bound long wave (e.g. Van Dongeren et al., 2007) and therefore a growth of IG waves, the rate of which lies between conservative shoaling (the growth in height due to the conservation of the energy flux when IG waves slow down in decreasing water depths, also referred to as Green's Law), $h^{-1/4}$ and the equilibrium solution of Longuet-Higgins and Stewart (1962) ($h^{-5/2}$). Laboratory observations show this phase shift to be frequency dependent, with either a larger phase lag and consequent growth of the lowest (De Bakker et al., 2013) or highest (Battjes et al., 2004) IG frequencies, the reason for these contradictory findings being as yet unclear. Battjes et al. (2004) established that this bound wave shoaling mechanism is dominant under a mild slope regime, which occurs when the normalized bed slope parameter β_b (see Eq. (2)) is typically below 0.3.

$$\beta_b = \frac{h_x}{\omega}\sqrt{\frac{g}{h}} \quad (2)$$

In this equation, h_x is the bed slope, ω is the angular frequency, g is the gravitational acceleration, and h is the depth at the mean breakpoint position. For typically $\beta_b \geq 1$, a steep-slope regime prevails and the growth of IG waves due to this first mechanism is weak while the breakpoint mechanism becomes dominant (see Section 2.2).

The depth-limited breaking of the individual short waves leaves to a shorward reduction in the wave-group envelope. As they are no longer bound to the group, IG waves are released and propagate as free waves (e.g. Masselink, 1995; Janssen et al., 2003; Battjes et al., 2004). Based on several laboratory datasets, Baldock (2012) questioned this simple release mechanism and proposed that it is only valid if the short waves are in the shallow water regime around the breakpoint (i.e. $kh < 0.3$). Conversely, Baldock (2012) proposed that the long bound wave may suffer a substantial dissipation when the short-wave breaking commences in intermediate water depth, which rather occurs under short-period waves and/or storm conditions.

2.2. Moving breakpoint

In addition to the creation of a bound wave, the groupiness of the incident short waves also causes the position of the short-wave breakpoint to vary in time on the timescale of the wave groups, as the higher short waves break further offshore than the lower ones. The time-variation of the breakpoint position causes a time-variation of the radiation stress gradient in the zone of initial breaking, which is balanced by a time-variation of the wave set-up.

The first analytical approach to study this breakpoint mechanism and the related infragravity wave dynamics was performed by Symonds et al. (1982), who considered the depth-integrated, linearized shallow water equations for the flow averaged over the incident short wave period, with a breakpoint position assumed to vary sinusoidally in time. This approach was restricted to normally-incident waves on a beach with a constant slope, and used a constant short wave height-to-water depth ratio $\gamma_b = H_b/h$ (the so-called "breaking index"), where H_b and h are respectively the short wave height and the water depth at initial breaking. Fig. 3 shows a schematic representation of the cross-shore variation of the minimum, mean and maximum wave height related to the incident wave groups, as well as the associated (steady state) set-up modulation. According to this approach, the wave groupiness should vanish in the surf zone. However, List (1991) showed that wave groups can in fact persist into the surf zone. When focusing only on the free wave solutions resulting from the breaking of the incoming waves (i.e. neglecting the forced bound wave outside the surf zone in the equations) and considering that there is a substantial shoreline reflection, Symonds et al. (1982) found that a standing infragravity wave forms shoreward of the breaking zone while an outgoing progressive infragravity wave exists seaward of this forcing region. Since free infragravity waves are radiated away from the breaking zone in both the

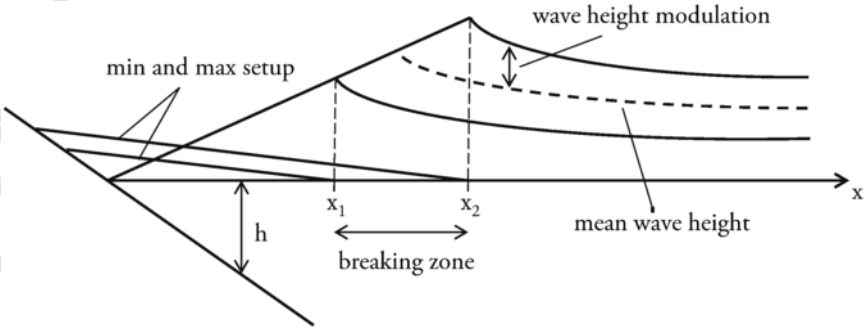

Fig. 3. Schematic representation of the cross-shore variation of the minimum, mean and maximum short wave height, with the associated steady state set-up through the surf zone. x_1 and x_2 are the minimum and maximum positions of the breakpoint, and h is the water depth. (Figure reproduced from Symonds et al. (1982).)

onshore and offshore direction, the resultant outgoing wave outside the surf zone is the sum of the seaward radiated wave and the initially shoreward radiated wave once reflected at the shore. Therefore, the amplitude of this resultant infragravity wave depends on the relative phase between the two free waves propagating seaward.

Later on, a more comprehensive approach was proposed by Schäffer (1993) who included a forcing term in the depth-integrated, linearized shallow water equations, thus taking into account the incident bound wave in the solution along the cross-shore direction. Moreover, the breakpoint mechanism is handled in this study with a hybrid method combining the approach of Symonds et al. (1982) with a treatment of the breakpoint position that allows the propagation of the wave groupiness into the surf zone. The resulting solution corresponding to the infragravity wave at the group frequency shows a gradual change from a standing wave at the shoreline to a seaward progressive wave offshore of the breaking zone. This result is generally in agreement with the results of Symonds et al. (1982), except that the nature of the infragravity wave changes more gradually between the two sides of the breaking zone because the equations account for the forced bound wave. This study also confirmed the roughly linear dependence between the infragravity wave amplitude at the shoreline and the offshore short-wave amplitude initially observed by Munk (1949) and Tucker (1950), and then by Guza and Thornton (1982, 1985).

The generation of free infragravity waves through this moving breakpoint mechanism has been partly confirmed by laboratory data (e.g. Baldock and Huntley, 2002), and by field experiments conducted on a sandy barred beach (Contardo and Symonds, 2013) and on a fringing coral reef (Pomeroy et al., 2012). As mentioned in the previous section, the relative importance of bound waves and breakpoint-generated waves was studied in more detail by Battjes et al. (2004) who concluded that the breakpoint forcing is expected to be dominant on steeper slopes (i.e. typically $\beta_b \geq 1$), while the bound wave shoaling mechanism (see Section 2.1) should be more important on milder slopes (i.e. typically $\beta_b \lesssim 0.3$). This is in agreement with List (1992), Van Dongeren et al. (2002) and De Bakker et al. (2015b), who found that the bound wave appears only weakly enhanced on a relatively steep slope because of ineffective, time-limited energy transfer from the short waves to the IG wave during shoaling. Baldock and Huntley (2002) proposed that the relative importance of the breakpoint mechanism may be greater for storm conditions (i.e. steep incident short-period waves), than for milder long-period swell waves.

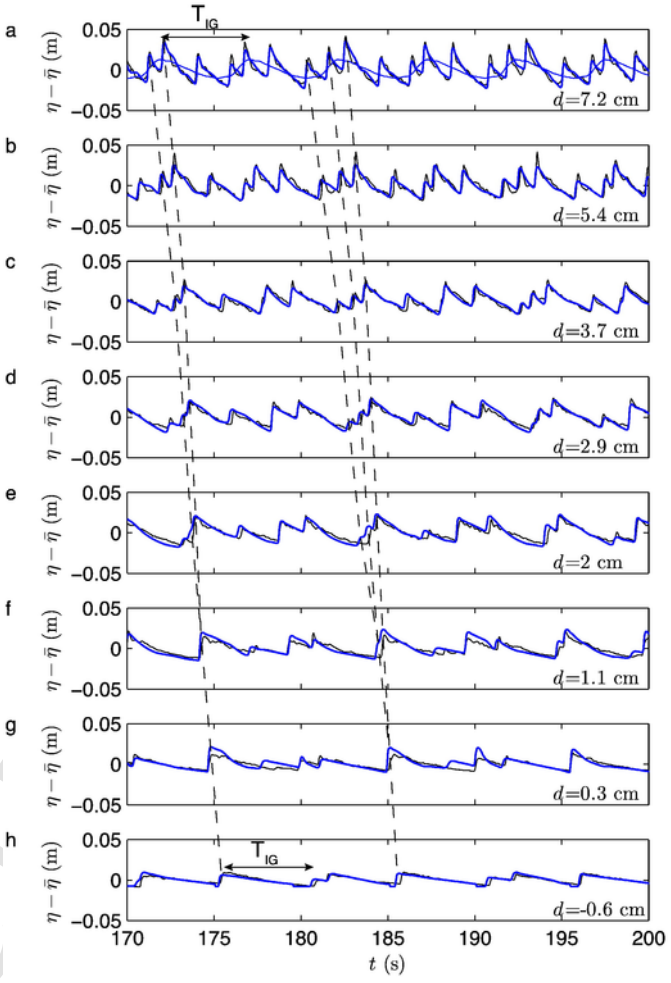

Fig. 4. Modelled (thick blue lines) and measured (thin black lines) surface elevation time-series at different locations within the surf zone (still water depth varying between d = 7.4 cm (a) to -0.6 cm (h)) for the bichromatic wave case A-1 from van Noorloos (2003) lab experiment. The model results were obtained using a shock-capturing NSWE model (Marche et al., 2007) forced using the measured time-series at d = 8.9 cm (see also Tissier et al. (2017)). The thin blue line on panel (a) is the low-frequency component of the modelled surface elevation time-series. The horizontal arrow indicates the IG wave period T_{IG} for this bichromatic wave case.

2.3. Bore merging

After breaking, short waves reorganize themselves in the inner surf zone into bores (breaking wave front, resembling to a hydraulic jump). For random wave fields, the difference in celerity between consecutive bores, which will be explained below, can lead to the confluence of the wave fronts. When the inner surf zone is large enough, a bore can overtake the bore ahead and merge together into a single wave front (see Fig. 4). This nonlinear process leads to an increase in the wave period in the surf zone, and as such contributes to an energy transfer from short wave frequencies to IG wave frequencies.

Bore merging was commonly observed in the field (Huntley and Bowen, 1975; Huntley and Bowen, 1974; Bradshaw, 1980; Sénéchal et al., 2001b), but very few studies have analysed this phenomenon in detail. Early field observations (Huntley and Bowen, 1975; Huntley and Bowen, 1974; Bradshaw, 1980) suggested that bore merging occurs more frequently in the surf zone of gently sloping beaches than on steeper beaches. This slope dependence was confirmed in the laboratory by Mase and Iwagaki (1984), who calculated the ratio of the number of wave crests running-up the beach to the number of incident wave crests for a series of irregular wave experiments. They showed that the number of waves running-up at the beach decreases as the surf similarity parameter (Iribarren and Nogales, 1949) decreases, i.e. they observed a stronger frequency down-shift on gently sloping dissipative beaches (see also Mase, 1989). The work of Sénéchal et al. (2001a,b) is one of the few attempts to quantify the modification of the wave field associated to bore merging in a natural surf zone. They observed a significant increase of the mean period in the inner surf zone of their gently sloping beach (+30% at their shallowest location). The longest waves recorded by Sénéchal et al. (2001a) in the inner surf zone had periods greater than two times the mean offshore period, and were within the IG wave band. This suggests that, for these wave conditions, bore merging leads to a weak increase of the energy in the IG-frequency band.

Bore merging is generally associated with the phenomenon of amplitude dispersion, i.e. the fact that larger bores propagate faster and will eventually catch up with the smaller ones if they are given enough time (e.g., Sénéchal et al., 2001a; Brocchini and Baldock, 2008). Over a gently sloping beach, however, wave grouping is expected to decrease due to breaking over the wide surf zone, and additional mechanisms may play a significant role. Based on the analysis of several laboratory datasets, Van Dongeren et al. (2007) and Tissier et al. (2015) suggested

that IG waves could be important for bore merging. More specifically, Tissier et al. (2015) showed that the intra-wave variability in celerity observed in their laboratory surf zone could largely be explained by the IG-wave induced modulation of the water level and velocity field (waves riding on the IG wave crests propagate faster than those riding on the IG wave troughs, see also Fig. 4a). Moreover, they found that the location at which bores start merging correlates with the relative IG wave height.

In the surf zone of gently sloping beaches, frequency-dispersion is weak and wave dynamics can be well described by the nonlinear shallow water equation (hereafter NSWE) (e.g., Bonneton, 2007; Hibberd and Peregrine, 1979). Following the concept of weak-solution (Whitham, 1974), the broken-wave fronts can be approximated by discontinuities or shocks. For non-periodic wave forcing, shocks propagate with different celerities. This is due to both the shock strength variability (i.e. amplitude dispersion) and, as discussed above, to the presence of IG waves. A high-celerity shock can overtake the shock ahead and coalesce into a single shock (Peregrine, 1974). Numerical non-linear shallow water equations (hereafter NSWE) simulations based on shock-capturing schemes show that this theoretical framework gives good results in comparison with both field data (Bonneton and Dupuis, 2001) and laboratory data (see Fig. 4).

Field and laboratory observations clearly show that bore merging is a ubiquitous phenomenon in the inner surf zone of gentle dissipative beaches. This nonlinear process induces a reduction of wave frequency across the surf zone and thus participates in an energy transfer from short waves to low frequency waves. However, this process seems to be a less dominant mechanism for IG wave generation (see Tissier et al., 2017) compared to the bound wave and the moving breakpoint discussed above. Bore confluence and subsequent merging are strongly influenced by the IG wave field generated outside the inner surf zone. The strong non-linear interactions between localized wave fronts and IG waves and their consequences in terms of spectral representation are not fully understood and should be more closely examined.

3. Propagation and transformation

3.1. Energy transfers

Several field and numerical modelling studies have observed that during propagation towards the shore, IG waves exchange energy not only with the short-wave band but also within the IG frequency band itself (Thomson et al., 2006; Henderson et al., 2006; Ruju et al., 2012; Guedes et al., 2013; De Bakker et al., 2015b; Fiedler et al., 2015). On steep beaches or in the outer surf zone of mild sloping beaches, IG wave heights are relatively small compared to the short-wave heights. Here, IG waves interact with the short waves (particularly around the energy spectral peak), and the energy at IG frequencies is spread to a wide range of high frequencies (Ruju et al., 2012; De Bakker et al., 2015b). On the contrary, on gently sloping beaches, IG waves are relatively more important compared to short waves and are interacting predominantly with themselves, thereby creating higher IG harmonics and inducing the IG wave shape to change to asymmetric. To illustrate these energy transfer trends, the imaginary part of the bispectra of wave field simulations over both a steep and a mild slope are shown in Fig. 5. Colours indicate direction of the energy transfers, and colour intensity is a proxy of the magnitude of the energy transfers. Positive values at B_{f_1,f_2} indicate a transfer from f_1 and f_2 to f_3, the sum frequency. Negative values indicate a transfer from f_3 to both f_1 and f_2. For an introduction to bispectral analysis please see Appendix B. On the steep slope, two interaction patterns dominate during the decrease in IG-wave energy (Fig. 5a).

One is the negative band ranging from about $B(0.22,0.22)$ to $B(0.44,0)$, where energy is transferred from the spectral peak to frequencies lower than the spectral peak, including IG frequencies. The other is a positive band ranging from $B(0.44,0)$ to $B(0,44,0.44)$ where energy is transferred to frequencies higher than the spectral peak by interactions between the spectral peak and frequencies lower than the spectral peak, including IG frequencies. The positive band ranging from $B(0.44,0)$ to $B(0,44,0.44)$ in the bispectra (Fig. 5a) dominates over the negative band ranging from about $B(0.22,0.22)$ to $B(0.44,0)$, leading to IG wave energy decrease. On the contrary, in the surf zone of gently sloping beaches, or in the inner surf zone of mild sloping beaches, interactions involving short wave frequencies have already disappeared entirely and the wave field is dominated by IG wave energy. Here, the bispectrum is dominated by IG-IG interactions (Fig. 5b), leading to the development of IG harmonics, and the steepening of the IG wave close to shore (see Section 3.2).

3.2. Dissipation

Since the late 1990s, several field (e.g., Ruessink, 1998a; Sheremet et al., 2002; Henderson et al., 2006; Guedes et al., 2013; De Bakker et al., 2014; Inch et al., 2017a; Fiedler et al., 2015), laboratory (e.g., Battjes et al., 2004; Van Dongeren et al., 2007; De Bakker et al., 2015a) and numerical modelling(e.g., Van Dongeren et al., 2007; Ruju et al., 2012; De Bakker et al., 2015b) studies have observed that IG-wave energy may decrease considerably near the shoreline. Research

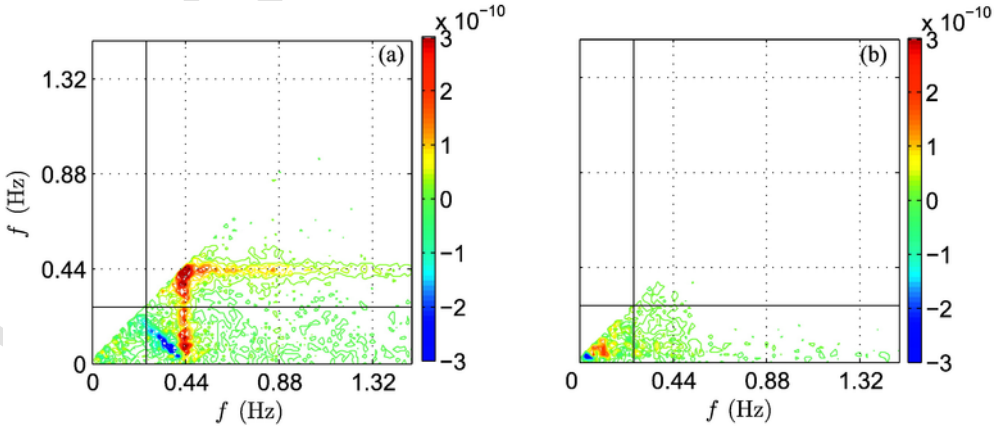

Fig. 5. Imaginary part of the bispectrum in m^3 (x 10^{-6}) of the incoming wave signal (η^+) for a narrow-banded wave condition over (a) a 1:20 slope and (b) a 1:50 slope in a water depth h of 5 cm (equal to h = 1 m in the field) for values where $b^2 > b_{95\%}$. Dashed lines indicate the spectral peak (f = 0.44 Hz) and its higher harmonics and the solid lines correspond to the frequency cutoff between IG waves and short waves. After: De Bakker et al. (2015b)

conducted in the swash zone also observed energy dissipation at IG frequencies, as swash excursion did not increase with more energetic offshore wave conditions, indicating saturation (e.g., Ruessink et al., 1998b; Ruggiero et al., 2004; Sénéchal et al., 2011; Fiedler et al., 2015). The first study that attempted to explain the source of IG wave energy loss proposed bottom friction as the dominant dissipation mechanism (Henderson and Bowen, 2002). Later studies showed that bottom friction is too low on sandy beaches to account for large IG wave energy losses, and is therefore now considered only as a secondary dissipation mechanism (Henderson et al., 2006; Van Dongeren et al., 2007; Lin and Hwung, 2012; Van Dongeren et al., 2013; De Bakker et al., 2014). On the contrary, for coral reefs, where the friction coefficient is one order of magnitude larger ($c_f \approx 0.02$ –0.05) than on sandy beaches, bottom friction is currently considered as the main cause for IG-wave energy loss (Pomeroy et al., 2012; Van Dongeren et al., 2013). It is now clear that, on sandy beaches, part of the energy loss at IG frequencies is not directly dissipated, but is transferred away from the IG band. On rather steep slopes, it is transferred back to short wave frequencies, whereas on gentle slopes it is transferred to higher IG harmonics, of which a part may reach into the short-wave band (see Section 3.1). The development of IG harmonics leads to wave shape change to skewed (peaked wave crests and longer wave troughs) and asymmetric (saw-tooth shaped), and leads to the steepening of the IG wave. Laboratory and field observations on gently sloping beaches (1: 35–1:80) observe this wave shape change and identify particularly strong dissipation close to the shoreline, suggesting breaking as the dominant dissipation mechanism (Battjes et al., 2004; Van Dongeren et al., 2007; Lin and Hwung, 2012; De Bakker et al., 2014; De Bakker et al., 2015a). This phenomenon is supported by observations of bore-like IG waves in laboratory experiments of Nazaka and Hino (1991) and Van Dongeren et al. (2007), and numerical modelling by Ruju et al. (2012) and De Bakker et al. (2015b).

3.3. Reflection

Any variation of the properties of the medium in which waves propagate, such as the currents or the water depth, will cause partial wave reflections. These partial reflections become significant when the variations of the medium properties are large for the representative wavelength, which is particularly true for IG waves in coastal waters. The interaction between the incident and the reflected waves gives rise to a standing (or stationary) wave pattern, which, for a normally incident monochromatic wave, can be expressed as:

$$\begin{aligned}\eta(x,t) &= \eta_i(x,t) + \eta_r(x,t) \\ &= a_i \sin(\omega t - kx) + a_r \sin(\omega t + kx)\end{aligned} \tag{3}$$

where a_i and a_r correspond to the amplitudes of the incident and reflected waves, respectively. If 100% of the incoming wave energy is reflected (such as against a vertical wall), $a_i = a_r = a$ and

$$\eta(x,t) = 2a \sin(kx)\cos(\omega t) \tag{4}$$

which corresponds to a standing wave of amplitude $2a$ with nodes at locations $x = (1/4)\lambda + (n/2)\lambda$ (where n is an integer) and antinodes at locations $x = (n/2)\lambda$. When the reflection is not total ($R = a_r/a_i < 1$), the resulting wave is a partially standing wave, which can be written as the sum of a progressive wave and a fully standing wave:

$$\eta(x,t) = (a_i - a_r)\sin(\omega t - kx) + 2a_r \cos(kx)\sin(\omega t) \tag{5}$$

The pioneering work of Tucker (1950) on IG waves (which they referred to as "surfbeat" at that time) was probably the first to mention the reflection of IG waves at the coast. Several studies followed (e.g. Huntley et al., 1981; Suhayda, 1974) and demonstrated that IG waves were predominantly standing in the cross-shore direction. The seminal study by Guza and Thornton (1985) was one of the first to indicate the frequency dependence of IG wave reflection, with standing waves at $f < 0.03$ Hz but an increasingly progressive wave pattern for higher frequencies, with $R \approx 0.5$. Elgar et al. (1994) analysed measurements from an array of bottom-mounted pressure sensors in 13 m water depth, 2 km off Duck beach, North Carolina, where the beach slope varies between 0.05 and 0.14, depending on the tidal stage. Seaward of the surf zone, the measured ratios of seaward to shoreward IG wave energy (R^2) were between 0.5 and 3.0, indicating that IG waves were gaining energy in the surf zone, before being reflected from the steep beach face. They also demonstrated that R^2 increased with offshore swell energy. Using collocated pressure and velocity sensors deployed between 1 and 6 m water depth over a gently sloping beach, Sheremet et al. (2002) decomposed the IG wave field into shoreward and seaward propagating components. They showed that the cross-shore seaward energy flux was locally larger than the shoreward energy flux, with cross-shore variation of R^2 ranging from 0.4 to 1.5. At the shoreline, a R^2 close to one indicated strong IG wave reflection. Tidal modulation of R^2 outside of the surf zone was reported by Okihiro and Guza (1995), with higher reflection occurring at high tide when the beach slope was steeper. More recently, however, a study by Thomson et al. (2006) observed almost full shoreline reflection at both high and low tides. These authors attributed tidal modulation of the reflected IG energy flux offshore to surf zone modulation of the incident energy flux. Henderson et al. (2000) investigated the frequency dependant cross-shore IG wave pattern further by performing a frequency-domain EOF (Empirical Orthogonal Functions) analysis of the pressure fluctuations in the IG band. They observed a clear nodal structure at the lowest IG frequencies with phase jumps of ± 180° at the nodes, typical of cross-shore standing waves and strong reflection. In contrast, higher IG frequencies displayed partial standing or progressive wave patterns along with an approximately linear, shoreward increase in phase difference. While Henderson et al. (2000) did not investigate the mechanism responsible for the stronger dissipation of higher frequency IG waves, it is likely that this behaviour is related to depth-induced breaking, as explained in Section 3.2

These results were recently corroborated by De Bakker et al. (2014) who analysed near-bed pressure and velocity measurements on a 1:80 and a 1:30 sloping beaches in The Netherlands.

Laboratory observations from Battjes et al. (2004) showed that the heights of the incident and reflected low frequency IG waves were approximately equal, indicating almost full shoreline reflection, whereas the reflected wave height of higher frequency IG waves was around one third of the incident wave height. They attributed these lower R (the ratio between the outgoing and incoming IG wave height) values to the breaking of the higher-frequency subharmonic waves (see Section 3.2). In order to quantify the conditions where reflection was prevailing, these authors defined another normalized bed slope parameter, β_H, defined as

$$\beta_H = \frac{h_x}{\omega}\sqrt{\frac{g}{H}}, \tag{6}$$

where, unlike in Eq. (2), H corresponds to the height of the incoming IG wave. According to the same authors, the prevalence of IG wave reflection is controlled by β_H, where large reflection occurs under a steep slope regime ($\beta_H > 1$) while lower reflection occurs under a mild slope regime ($\beta_H < 1$). A follow-up study by Van Dongeren et al. (2007)

based on bichromatic wave experiments and numerical modelling (Delft3D-Surfbeat model, (Roelvink, 1993)) showed that the frequency dependent reflection coefficient R at the shoreline was related to β_H (Eq. (6)) with a transition at $\beta_H \approx 1.25$, above which $R \approx 1$ (steep-sloping regime) and, below which wave breaking yielded lower R values (mild-sloping regime, see Section 3.2) (Fig. 6). These results were corroborated by Ruju et al. (2012), who used the phase-resolving Reynolds Averaged Navier–Stokes model IH-2VOF (Lara et al., 2010) to investigate the low-frequency energy balance in the surf zone for bottom slopes ranging between 1:20 and 1:30.

However, several field experiments (e.g. De Bakker et al., 2014; Inch et al., 2017a) suggested that the transition between steep slope and mild slope regimes occurs for substantially larger β_H, typically around 3. The different transition values found by these authors are likely due to the cross-shore locations chosen to compute the shoreline reflection coefficient. Indeed, De Bakker et al. (2014) and Inch et al. (2017a) estimated R within the inner surf zone rather than at the shoreline, since measurements on the edge of the swash zone are almost impossible to collect in the field, especially when using an array of pressure sensors to estimate reflection. Also, Van Dongeren et al. (2007) used laboratory bichromatic wave experiments, where the transition region is expected to be stable, whereas De Bakker et al. (2014) and Inch et al. (2017a) investigated natural beaches under irregular wave fields, where the transition region is expected to vary in space and time. De Bakker et al. (2013, 2014) observed bulk squared IG reflection coefficients $R^2 \approx 0.1$ at the shoreline of a low-sloping laboratory beach with random wave conditions. EOF analysis of the IG sea-surface elevations demonstrated a well-developed standing wave pattern at low IG frequencies, corresponding to $R^2 \approx 0.5$, whereas high frequency IG waves were predominantly onshore progressive.

Rijnsdorp et al. (2015) applied the phase-resolving wave model SWASH (Zijlema et al., 2011) to a natural beach and showed that SWASH tends to underpredict the IG reflection coefficient, but still revealed its frequency dependent behaviour with near-zero (respectively near-perfect) reflection for high (respectively low) frequency IG waves.

Finally, Inch et al. (2017b) showed that any uncorrelated signal in sensor arrays (see Appendix A) can lead to an overestimate of the correlation coefficient. Although correctable, this potential bias in R has not been accounted for in many prior studies.

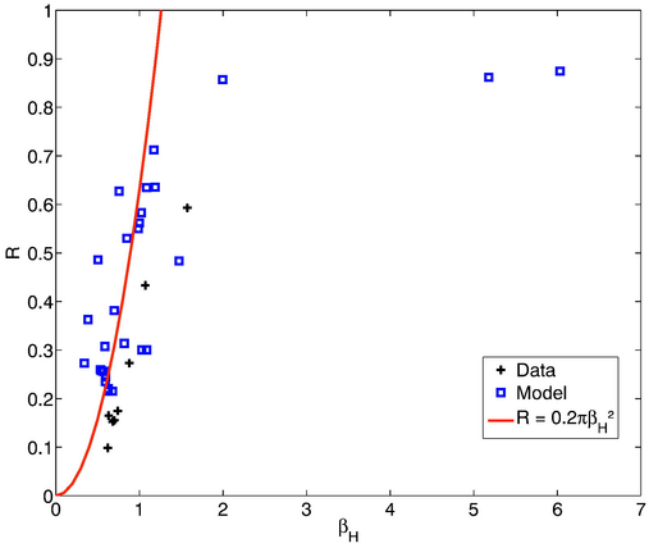

Fig. 6. Relations between the reflection coefficient R and the normalized bed slope parameter β_H, modified from Van Dongeren et al. (2007).

3.4. Edge waves

The reflection of infragravity waves at the shoreline, described in Section 3.3, can lead to refractively trapped motions which could turn into periodic alongshore-travelling patterns, also referred to as edge waves. Edge waves are freely propagating, alongshore periodic waves that are trapped to the coast on one side by reflection from the shoreline and on the other side by refraction over a sloping bathymetry. Leaky waves represent the companion to edge waves but do not return to the coast by refraction; instead, they escape to deep water. While edge waves are standing in the cross-shore direction, their alongshore behaviour is usually progressive. Early models of edge wave formation date back to Stokes (1846) and Eckart (1951), with several further refinements provided in more recent years. The mechanism leading to the appearance of edge waves is related to a weakly resonant transfer of energy from reflected incident waves on a planar beach to edge wave perturbations. On a planar beach with slope β a discrete number of edge wave modes can exist, satisfying the dispersion relation (Eckart, 1951):

$$\sigma_e = g k_e^2 \sin(2n+1)\tan\beta, \tag{7}$$

where σ_e and k_e are the radian frequency and alongshore wave number of the edge waves, g is gravitational acceleration, and n is the edge modal number, which corresponds to the number of zero-crossings (nodes) in the cross-shore direction before the final amplitude decay at the turning point. Mode 0 edge waves ($n = 0$) have, for a given T_e, the largest alongshore wave number. With an increase in n, the wave number decreases (i.e., the alongshore wave length increases) up to point where $k_e = \sigma_e^2/g$, the deep-water wave number. The edge wave mode that satisfies this relation is called the cut-off mode. For $k < \sigma^2/g$ a continuum of leaky waves exists. Edge waves have their largest amplitude at the shoreline and a cross-shore amplitude function $\Phi_n(x)$ that on a planar beach with slope β reads

$$\Phi_n(x) = \mathrm{e}^{-k_e x} L_n\left(k_e x\right), \tag{8}$$

where L_n is the Laguerre polynomial of order n. Analytical expressions for $\Phi_n(x)$ also exist for an exponential beach profile, but numerical approaches must be used for more complex beach profiles (Holman and Bowen, 1979). Solutions for such beach profiles are generally remarkably different from the analytical expressions for similarly sloping linear beaches, highlighting the profound effect of, for example, sandbars and troughs on cross-shore edge-wave structure.

Observations indicate that steep and gently sloping beaches have different edge-wave periods. On steep, reflective beaches, two types of edge waves are considered likely to develop: synchronous and subharmonic, with periods the same or double the period of the incident wave field, respectively, and accordingly, these edge waves are not necessarily in the IG frequency band. In line with theoretical findings, laboratory experiments conducted under normally approaching monochromatic waves have conclusively shown that subharmonics of mode 0 are the most easily excited edge wave mode (Guza and Davis, 1974). On more gently sloping beaches, wave breaking is sufficiently strong to dampen the above-mentioned resonant transfer and, as a result, synchronous and subharmonic edge waves do not form. Instead, edge waves have substantially larger periods than the incident waves. These IG edge waves are likely the result of the bound long wave, generated as explained in Section 2.1. As pointed out by Herbers et al. (1994), a pair of short-wave components with frequencies and vector wave numbers (f_1,k_1) and (f_2,k_2), where $f_2 > f_1$, excite a secondary bound wave

with difference frequency and vector wave number ($f_2 - f_1$,$k_2 - k_1$). During release, the wave number of vector of the free IG waves equals the difference in vector wave numbers of the two forcing waves. Because $|k_2 - k_1|$ is much smaller than k_1 and k_2, even moderate obliquity in the short waves already results in large IG propagation angles with respect to the shoreline. Consistent with observations, the IG wave field is thus directionally far broader than is the incident wave field. This also implies that, especially on gently sloping wide shorefaces and shelves, the vast majority of IG motions will become edge rather than leaky waves (Herbers et al., 1995).

IG edge waves are ubiquitous in the surf and swash zones of gently sloping beaches, and their characteristics have been studied extensively using alongshore arrays of current meters or videoed swash motions (e.g., Oltman-Shay and Guza, 1987; Howd et al., 1991; Oltman-Shay and Howd, 1993; Holland and Holman, 1999). The data are generally computed into frequency-alongshore wavenumber ($f - k_y$) spectra, which reveal concentrations of energy aligning with edge-wave dispersion lines for various n. For situations with approximately shore-normal incident waves, IG waves progress about equally in both directions along the coast, resulting in alongshore standing motions without alongshore reflectors. Considerable asymmetry in up- and downcoast edge waves arises in the case of obliquely incident waves. In the case of pocket beaches where lateral boundaries can induce strong reflection, edge waves are generally alongshore standing (Özkan-Haller et al., 2001). The breaking-induced alongshore currents also distort the dispersion curves and cross-shore amplitude function of the edge waves (Howd et al., 1992; Oltman-Shay and Howd, 1993). In particular, k_e increases (i.e., shorter wave lengths) and the nodal structure shifts landward for edge waves opposing the current, while the opposite happens for edge waves propagating with the current. Howd et al. (1992) modelled these effects by modifying the bottom profile into an effective profile, that is, the profile as felt by edge waves in the presence of the current. Finally, $f - k_y$ spectra computed from field (Bryan et al., 1998) and model (e.g., Rijnsdorp et al., 2015) data in the presence of sandbars reveal edge waves that are refractively trapped on the sandbar. These bar-trapped modes can arise when the edge-wave phase speed is between $\sqrt{gh_{\text{bar}}}$ and $\sqrt{gh_{\text{trough}}}$, where h_{bar} and h_{trough} are the effective water depth at the bar and in the trough, respectively. In Rijnsdorp et al. (2015)'s modelling study, the bar-trapped modes contributed up to 50% of total IG variance atop an approximately 3-m high outer bar during mild-wave conditions, but contributed substantially less during storm conditions with significant wave breaking on the bar. Bar-trapped modes were not predicted for the substantially less pronounced inner bar.

4. Impacts

4.1. Sandy beaches and dunes

4.1.1. Rip currents

Rip currents are spatially-concentrated seaward flows that extend from close to the shoreline, through the surf zone, and decay with offshore distance (MacMahan et al., 2006; Dalrymple et al., 2011; Castelle et al., 2016b), which are ubiquitous along wave-exposed coasts. They have been studied for almost a century (Davis, 1925), notably because they are a key driver for the transport and cross-shore mixing of sediment, heat, pollutants, nutrients and biological species (Talbot and Bate, 1987; Shanks et al., 2010; Sinnett and Feddersen, 2014) and because they represent an important coastal hazard. For instance, during severe storms they can drive localised beach and dune erosion (Thornton et al., 2007; Loureiro et al., 2012; Castelle et al., 2015; McCarroll et al., 2014). More recently, rip currents have been of both scientific and societal interest because they are now acknowledged to be the leading deadly hazard to recreational beach users with hundreds of drowning deaths and tens of thousands of rescues per year on beaches worldwide (e.g. Gensini and Ashley, 2009; Brewster, 2010; Arozarena et al., 2015; Castelle et al., 2016a).

Although IG waves may not fundamentally drive rip current formation, for some time they appeared as a relevant candidate to explain the presence of rip currents. Bowen (1969) and Symonds and Ranasinghe (2000) demonstrated that interactions between the short-wave groups and synchronous standing IG edge waves (Section 3.4) could force rip currents. In the former paper, the mechanism is that the alongshore variation in total water levels would lead to an alongshore variation of wave heights, and thus in set-up, and rip current would occur at the minimum of the set-up. In the latter paper, the assumption of alongshore variation of the wave heights and the set-up was released and a mechanism presented in which the slow alongshore modulation of the water levels could force rip currents. However, rip currents are part of the nearshore circulation caused by the action of breaking short waves, and their development does not theoretically require the presence of IG waves. Rip currents on natural beaches show a considerable variability in terms of occurrence and location along the beach, owing to the variability of driving mechanisms (see Castelle et al., 2016b, for a review). Rip currents are generally caused by the alongshore variability of breaking wave height, which can arise from a number of causes, such as wave energy focusing enforced by offshore wave refraction (Long and Ozkan-Haller, 2005). Other mechanisms were also proposed, such as shear instability of the longshore current (Ozkan-Haller and Kirby, 1999), deflection of the longshore current against an obstacle (Castelle and Coco, 2013) and vorticity injected with the passage of individual breaking waves evolving into migrating surf-zone eddies (Feddersen, 2014). Since it is not possible to elaborate on the influence of IG waves on all rip types, we focus here on bathymetrically-controlled rip currents, which are driven by the alongshore variation in depth-induced wave dissipation. This type is the most common worldwide, together with rips controlled by headlands and coastal structures, and are found along oceanic, sea and lacustrine coasts.

IG waves affect the temporal behaviour of rip currents (e.g. Sembiring et al., 2016). Many field studies showed that rip flow kinematics can be partitioned into mean, IG (25–250 s) and very low frequency (4–30 min, VLF) components, with the tide further modulating rip flow velocity (e.g. MacMahan et al., 2006; Austin et al., 2010; Bruneau et al., 2014). MacMahan et al. (2004) used field data to show that rip current pulsations at IG frequencies are linked to standing IG motions but not to the ponding and subsequent release of water by wave group pumping. This stimulated the development of nearshore models addressing wave-driven currents at the scale of wave groups (e.g. Reniers et al., 2004; Roelvink et al., 2009), which were found to explain up to 80% of the IG wave height and 70% of the IG velocities observed on a rip-channelled beach (Reniers et al., 2006). Rip current pulsing and resulting eddies detaching from the rip were found to be an important exit mechanism of floating material from the surf zone towards the inner shelf (Reniers et al., 2009). Accordingly, IG waves do not affect mean rip flow patterns but strongly influence cross-shore and alongshore mixing (Fig. 7).

4.1.2. Ground water dynamics

Darcy's law states that, in isotropic porous media, water flows in the direction of decreasing potential (Darcy, 1856). This implies that any pressure gradient within a porous soil will induce a groundwater flow. In the context of sedimentary beaches, the key soil properties affecting the groundwater circulation are the hydraulic conductivity and the saturation, whereas in fractured rocks or reef environments, tortuosity and specific surface (Guyon et al., 2015) should also be taken into account. For the sake of simplicity, only the former case will be considered in this section.

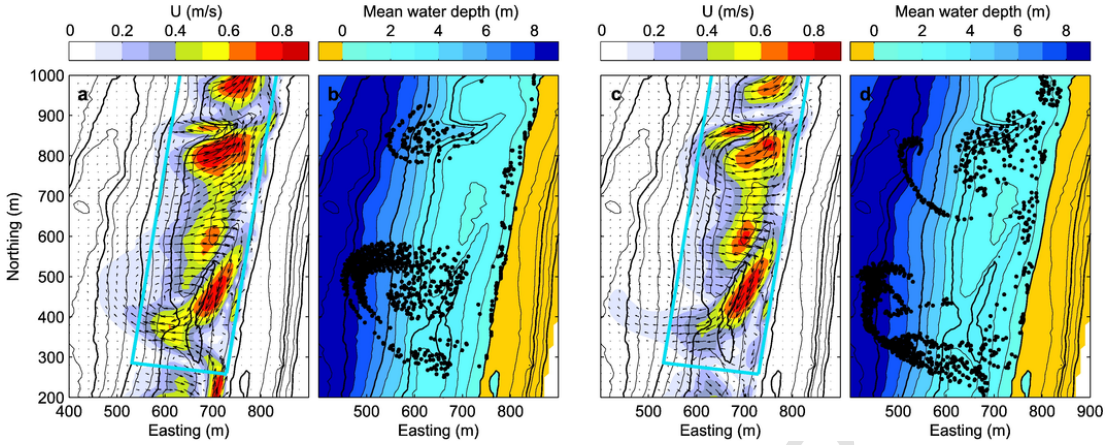

Fig. 7. Numerical modelling of wave-driven currents and passive drifter evolution at the rip-channelled beach of Biscarrosse, SW France (Bruneau et al., 2014) for summer wave conditions (Hs = 1 m, Tp = 10 s, shore-normal incidence) at a tidal level maximizing rip current activity (see for more detail on the modelling strategy in Castelle et al., 2016a). (a,c) Mean flow patterns with the colour bar and the blue box indicate velocity in m/s and the location of the initially seeded passive drifters, respectively. (b,d) Drifters (black bubbles) after 20 min of simulations. Left-hand and right-hand panels are without and with wave-group-forced IG motions, respectively.

In the permanently submerged zone, extending from deep water to the end of the inner surf zone, IG waves impact the groundwater dynamics mainly through: (i) the fluctuations of pressure at the sea bed interface driven by the IG content, and (ii) the structure of the porous soil (possibly evolving through time). The former can be computed using, e.g., linear wave theory while the latter can be estimated from some soil properties (porosity, saturation, compaction, depth of the porous layer, etc.) using models of pore-pressure transmission in homogeneous soils (Sakai et al., 1992). In the context of sedimentary beaches, poro-elastic soil theories reveal the importance of encapsulated gas in the sand, even for the small gas contents (a few percent) observed in the superficial layer (0.5-1 m) of intertidal sands (Bonjean et al., 2004). Pressure waves applied on the sea bed are both attenuated and phase shifted when propagating within the soil, which induces the development of vertical pressure gradients (Michallet et al., 2009). These processes are strongly dependent on wave frequency: the longer the wave, the stronger the groundwater pressure oscillation. This effect is quantified, among others, in poro-elastic soil models (Sakai et al., 1992). The related cyclic vertical flows, upward exfiltration under the wave trough and downward infiltration under the crest, are at most of the order of 0.01 mm/s for typical surf zone IG waves. Horizontal groundwater flows associated with free surface gradients of IG waves are two to three orders of magnitude smaller.

A much more substantial IG wave impact is expected around the beachface. Subterranean fluxes through sandy beaches have recently been the focus of an increasing interest due to their implication in the exchanges of fresh/salt water between ocean, coastal aquifers and lagoons (Burnett et al., 2006; Geng and Boufadel, 2015), the transport of nutrients or pollutants (Anschutz et al., 2009; Sawyer et al., 2014) and biogeochemical processes (McAllister et al., 2015). The effect of IG waves on groundwater dynamics is more important on sandy dissipative beaches, where IG waves usually dominate the dynamics. A first important parameter is the degree of saturation of the beach. While the sand bed in the lower part of the swash zone is expected to be permanently saturated, large IG-driven uprush events can reach unsaturated areas of the beach face, particularly during the rising phase of the tide and during storm surges. Complex dynamics develop under the beachface with asymmetric pressure fluctuations in the capillary fringe (Turner and Nielsen, 1997; Cartwright et al., 2006) and a hump-shaped watertable (Turner et al., 1997; Sous et al., 2013). However, due to the difficulty of performing direct and non-intrusive measurements in the sand soil, the characterization of pressure and saturation features within the vadose zone (located between the watertable and the beachface) remains a challenge and an active field of research (Horn, 2006; Heiss et al., 2015).

Inside the saturated part of the swash zone groundwater, periodic circulations are observed: exfiltration under the incoming uprush bore toe, infiltration during backwash. This pattern has been observed both for short wave driven swash (Li and Barry, 2000; Bakhtyar et al., 2011) and in the field for IG wave-dominated swash zone (Sous et al., 2016). The resulting time-averaged flow is a seaward groundwater circulation cell, with exfiltration/infiltration at the base/top of the swash zone (Turner et al., 2015; Sous et al., 2016). This flow pattern is illustrated in Fig. 8, which shows the measured groundwater head field and the resulting computed velocities driven by an IG wave event at the Rousty microtidal beach (SE France). Such circulation patterns are expected to be of great importance for mixing and exchange processes between ocean and beach aquifer. In the case of sandy beaches, the inland back-barrier watertable fluctuations (or related beach drainage systems) play a weak role on the swash groundwater dynamics (Turner et al., 2015). The possible effect of groundwater flows on bed stability and sediment transport has been an active field of research over the last decades to better understand the problem of swash zone morphodynamics (Turner and Masselink, 1998; Butt et al., 2001; Karambas, 2003). In the case of sandy beaches, seepage (in/exfiltration through the bed) velocities of about 0.1 mm/s are only able to affect a few percents of the relative sediment weight, so that the effect of through-bed flows is expected to be rather small compared to swash hydrodynamics (shear stress, turbulence, sediment load advected from the surf zone) and larger-scale morphodynamic processes. Further inland, the propagation of IG waves is rapidly damped by the low-pass filtering effect of the sandy beach (Nielsen, 1990; Turner, 1998).

On reflective gravel beaches, the effect of IG waves on beach groundwater dynamics is expected to be much weaker than that of gravity waves because the swash zone is mostly governed by swell and wind waves. However, compared to sandy beaches, swash infiltration occurs more rapidly (Steenhauer et al., 2011) leading to a net volume loss and a modification of the boundary layer structure (Butt et al., 2001). Finally, fluxes through the beachface are also more sensitive to inland watertable fluctuations (Lee et al., 2007; Turner and Masselink, 2012).

4.1.3. Run-up and overwash/overtopping

Wave run-up, defined as the set of maxima of the time-varying waterline elevation above the still water level, is the combined result of wave set-up in the surf zone and variance in the swash zone (i.e., wave

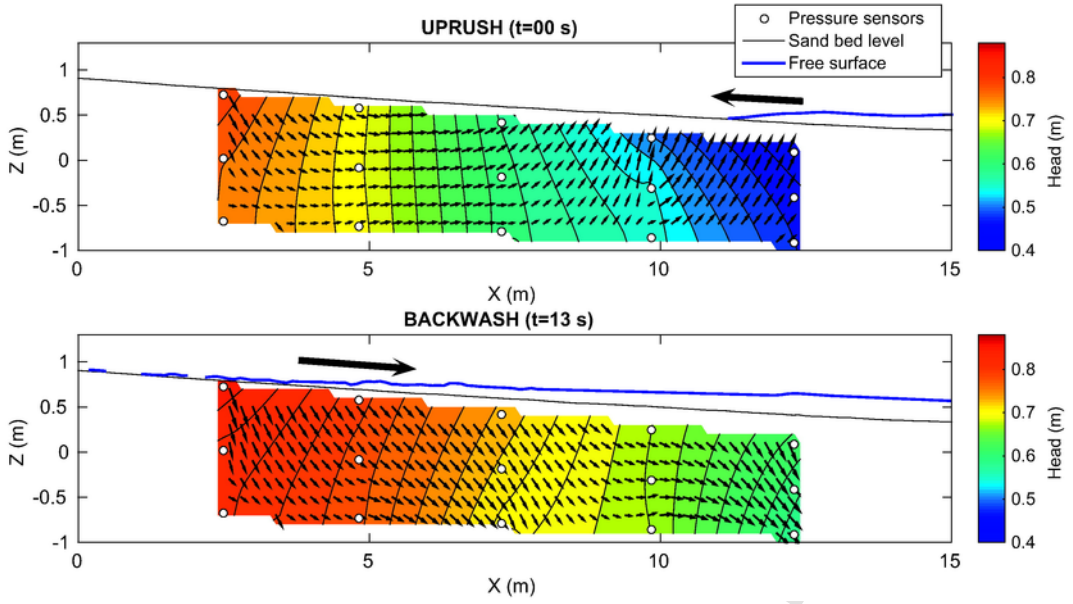

Fig. 8. Groundwater pressure head and velocity fields during uprush (top plot) and backwash (bottom plot) phases of an IG-driven swash event measured during the Rousty1412 field campaign in the Rousty beach (Camargue, France). The blue solid line indicates the free surface elevation measured by terrestrial LiDAR while the solid black line indicates the sand bed. Each white circle within the sand soil corresponds to a buried pressure sensor (5 Hz acquisition frequency). Colour contours indicate the groundwater head field, interpolated from measurements at each sensor. Vectors are groundwater velocities calculated from the head field using the Darcy's law.

uprush and backwash, Holman and Sallenger, 1985; Stockdon et al., 2006). On dissipative beaches, wave run-up is dominated by IG waves due to the saturation of the short-wave incident-band in the surf-zone (Guza and Thornton, 1982) and IG-band dominance at the seaward edge of the swash zone (e.g., Guza et al., 1984; Holman and Sallenger, 1985; Raubenheimer et al., 1996; Ruessink et al., 1998a; Ruggiero et al., 2001). Similarly, wave run-up on coasts fronted by coral reefs is often dominated by IG swash motions due to the dominance of IG-band and other low-frequency motions on the reef flat (e.g., Seelig, 1983; Nwogu and Demirbilek, 2010; Shimozono et al., 2015; Bricker and Roeber, 2015; Cheriton et al., 2016). However, even in cases without nearshore IG wave dominance, such as reflective sandy (e.g.,Vousdoukas et al., 2012; Blenkinsopp et al., 2016) and gravel (Almeida et al., 2015) beaches, IG swash motions may contribute substantially to wave run-up due to the saturation of the incident-band frequencies in the swash zone (i.e., uprush-backwash interaction between successive bores; Mase, 1995) and the persistence of wave groupiness into the swash zone (Baldock et al., 1997). On both dissipative and reflective beaches, the contribution of the IG-band to wave run-up is necessarily affected by the incident IG wave height seaward of the swash, and thus by the incident-band directional and frequency spread (Guza and Feddersen, 2012).

Overwash occurs when the run-up of individual swashes exceeds the height of the crest of a beach or island (Matias et al., 2012) and can cause flooding of the hinterland and erosion of coastal infrastructure. Despite the obvious societal importance of overwash with respect to flood safety and coastline management, relatively few studies have been carried out regarding overwash processes, and particularly the role of IG waves during overwash events.

Baumann et al. (2017) carried out measurements of overwash on a natural sandy dune under energetic wave conditions (H_s = 6.0m and T_p = 15s) combined with high spring tides. Fig. 9 shows that overwashes consist of bore-like asymmetric waves with periods ranging from 70 to 100 s. Such periods correspond to IG waves and the spectral analysis of the data revealed that energy in the short-wave band is almost nil. This strong dominance of IG waves in the beach upper part is related to the very dissipative morphology of the beach, in agreement with previous studies listed above.

McCall (2015) combined field measurements with numerical modelling at a steep, reflective, gravel barrier and showed that, although the majority of overtopping events were controlled by the short-wave band motions, large overwash events under low-freeboard (i.e. the height difference between the mean water level and the crest of the barrier) conditions were related to IG wave motions. Despite the scarcity of data, since overwash is an extension of the swash zone, it is generally expected that IG waves play a significant role in overwash conditions by increasing wave run-up and lowering overwash thresh-

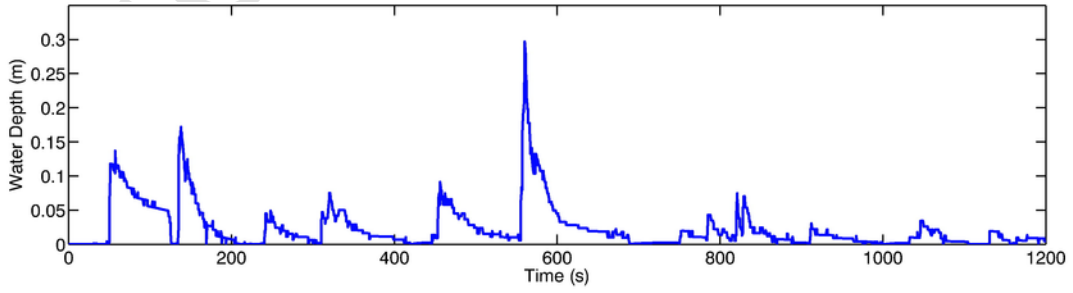

Fig. 9. Time series of water depth measured to the SW of Oléron Island (France) on 08/02/2016, showing overwash associated with IG waves with periods ranging from 70 to 100 s. Adapted from Baumann et al. (2017).

olds, and increasing the magnitude of the overwash discharge (e.g., Roelvink et al., 2009; McCall et al., 2010).

4.1.4. Sediment transport

Due to their important contribution to the surf- and swash zone hydrodynamics, IG waves have long been thought to play an important role in the sediment dynamics and subsequent morphological changes of sandy coasts (e.g., Bowen and Huntley, 1984; Wright and Short, 1984; Sallenger et al., 1985; Lippmann and Holman, 1990). The suspension and cross-shore transport of sand by IG waves have, therefore, been investigated in many studies (e.g. Abdelrahman and Thornton, 1987; Beach and Sternberg, 1988; Roelvink and Stive, 1989; Shibayama et al., 1991; Osborne and Greenwood, 1992; Russell, 1993; Aagaard and Greenwood, 1994; Aagaard and Greenwood, 1995; Ruessink et al., 2000; Smith and Mocke, 2002; Conley and Beach, 2003; Houser and Greenwood, 2005; Aagaard and Greenwood, 2008; Baldock et al., 2010; Alsina and Cáceres, 2011; Aagaard et al., 2013; Kularatne and Pattiaratchi, 2014; Pomeroy et al., 2015; De Bakker et al., 2016). However, the diversity in beach profiles and offshore wave conditions has created contrasting observations in direction and relative importance of cross-shore IG sand transport as well as the suspension mechanism.

Some studies observed that short-waves were the main sand stirring mechanism, whereas IG waves only advect this suspended sand either onshore or offshore (e.g. Larsen, 1982; Huntley and Hanes, 1987; Osborne and Greenwood, 1992; Ruessink et al., 1998a; Smith and Mocke, 2002). Based on hydrodynamic data, Abdelrahman and Thornton (1987) and Roelvink and Stive (1989) proposed a different hypothesis where the presence of the largest short waves at either the IG-wave trough (bound wave) or crest (free wave) could explain the timing of sediment suspension relative to IG wave phase, and the subsequent transport direction. This timing of suspension can be described by the correlation r_0 between the short wave envelope and IG motion. In the shoaling zone and outer part of the surf zone, larger (breaking) short waves are present at the IG wave trough (the IG wave can still be considered to be bound), and r_0 is negative. Consequently, net transports are directed seaward, as observed by for example Larsen (1982); Huntley and Hanes (1987); Osborne and Greenwood (1992); Ruessink (1998b); Smith and Mocke (2002). In addition, as water depths are lowered locally in the IG trough, short wave orbital velocities are larger close to the bed, by which the larger bed shear stresses can suspend even more sand there. In the inner surf zone, the larger short waves are present on the IG wave crest (the IG waves can be considered a free wave), and the correlation is positive. Due to the locally raised water levels, short waves can persist longer at the IG-wave crest than in the trough. Consequently, they suspend more sand at the IG-wave crest, providing a net shoreward transport at IG-wave timescale, as observed by, for example, Osborne and Greenwood (1992).

A second theory has been proposed by Aagaard and Greenwood (2008) who studied sand transport directions at two barred beaches, and observed transport directions to be related to the position with respect to a suspension maximum. These suspension maxima occur at positions with relative short wave height maxima (which at their sites typically occurs on upper seaward slopes or bar crests) where short waves suspend large amounts of sand while breaking. They observed a shoreward transport of sand by IG waves at the landward side of such suspension maxima, and a seaward transport on their seaward side of such maxima. Their theory may be related to the above-described correlation theory.

Other observations contradict these theories, as for conditions where IG waves dominated the water motion in the inner surf zone, the IG wave was seen to suspend sand as well (e.g. Beach and Sternberg, 1988; Russell, 1993). No preferential location of short waves could be distinguished for this data (r_0 would be nearly zero), and sand was mostly suspended under the IG trough, creating seaward directed sand transport.

Recently, based on measurements on both a gently ($\beta \approx 1{:}80$) and intermediately ($\beta \approx 1{:}35$) sloping beach De Bakker et al. (2016) proposed that the ratio of the IG-wave height with respect to the short wave height H_{IG}/H_{SW} could explain the previous contrasting observations. The H_{IG}/H_{SW} ratio would be a good parameter to estimate the type of stirring, and could also explain the resulting IG-wave sand transport direction and magnitude. On steeper sloping beaches, IG waves were relatively small and short waves dominated everywhere, HIG/HSW was typically lower than 0.4, and sand was suspended on the IG timescale by short waves. Here, the correlation between the short-wave group and IG orbital velocities determined whether IG-wave sand transport was seaward or shoreward (example in Fig. 10 a,c,e) directed. On average, the IG-wave component contributed for less than 20% to the total cross-shore transport. On the contrary, on the gently sloping beach, where IG waves dominated the water motion in the inner surf zone, the ratio HIG/HSW typically exceeded 0.4, and sand was suspended under onshore directed IG-wave velocities (example in Fig. 10 b,d,f). The resulting seaward IG transport contributed up to 60% of the total cross-shore transport.

Overall, steps have been made to extract a general trend behind IG sand suspension and cross-shore transport, but validation on other beaches is considered necessary, especially under storm conditions when the IG wave contribution to the total cross-shore transport can be substantial. Conducting experiments in large-scale flume facilities and extending phase-resolving models such as SWASH (Zijlema et al., 2011) with a sediment transport module could considerably add to this. The contribution of IG waves to longshore transport should also be investigated. The generic trends could then be implemented in a parameterized way in morphodynamic models used to asses coastal evolution.

4.1.5. Dune erosion and barrier breaching

IG waves are thought to be particularly important for beach morphodynamic response to storms, because the surf zone becomes saturated for short-wave band, but not for IG waves, and hence the inner surf zone and swash are dominated by low-frequency wave motions (e.g., Oltman-Shay and Hathaway, 1989; Raubenheimer and Guza, 1996). Roelvink et al. (2009) pointed out that high IG waves occasionally reach the dune front during storms and cause slumping (avalanching) of the wetted part of the dune face, which subsequently leads to avalanching of the dry dune. Through numerical modelling, they showed that this process plays an essential role in bringing sand from higher parts in the dune into the swash zone and further offshore from there. However, due to the inherent difficulty of separating interacting IG and short-wave dynamics, the precise role of IG waves on coastal morphodynamics during storms is difficult to prove using observational (laboratory and field) data. Instead of using observational data, Van Rijn (2009) and Van Thiel de Vries (2009) used calibrated process-based numerical models to investigate the effect of IG waves on dune erosion during storms. By turning on and off IG wave processes in numerical models, these studies proposed that IG waves may enhance dune erosion on a dissipative sandy coast by approximately 20–30% during extreme storm events.

Muller et al. (2016) simulated storm impact in the area of Les Boucholeurs (Western France), an area of marshland protected by relatively narrow dunes. Their modelling results suggest that, even in an area relatively sheltered from Atlantic swells, IG waves had an influence on the mean erosion of the dune crest, especially at the locations of the highest dunes. However, these authors found that the final position and geometry of breaches were not controlled by IG waves but by tide and surge overflow.

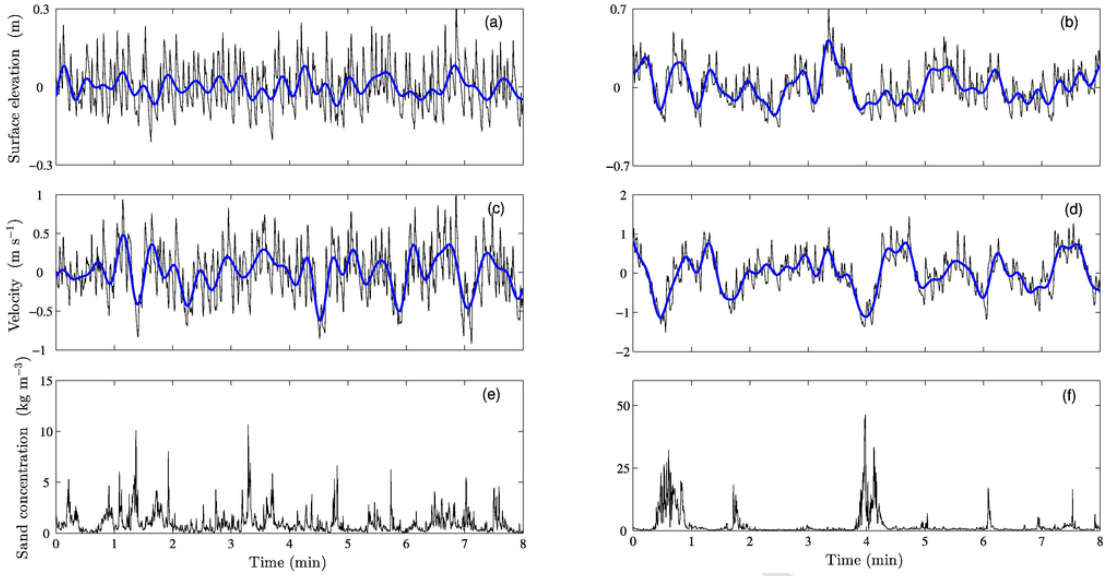

Fig. 10. Example timeseries of a positive correlation r_0 (a,c,e) in the inner-surf zone of the steeply sloping Zandmotor beach and a negative r_0 (b,d,f) in the inner-surf zone of the gently sloping Ameland beach. Please note the different y-axis scales. (a,b) sea-surface elevation (m) and (c,d) cross-shore velocity with in black the total velocity, and in blue the IG velocity, and (e,f) sand concentration. For Ameland location P11, $h = 1.00$ m, $r_0 = -0.04$, $H_{total}/h = 0.67$, $\bar{u} = -0.15$ m/s, $H_{IG}/H_{SW} = 1.00$. For the Zandmotor location P10, $h = 0.5$ m, $r_0 = 0.17$, $H_{total}/h = 0.66$, $\bar{u} = -0.16$ m/s, $H_{IG}/H_{SW} = 0.39$. After De Bakker et al. (2016).

The findings of the numerical model investigations discussed above can be placed in a more generalized context using the Storm Impact Scale of Sallenger (2000). The Storm Impact Scale relates the type of morphodynamic response of a natural sandy barrier island to the position of the swash zone during the storm (i.e., surge level plus wave run-up and wave run-down) relative to the elevation of the beach and dune. The four regimes in the Storm Impact Scale are: (1) the swash regime, related to beach erosion; (2) the collision regime, related to erosion of the seaward face of the dune; (3) the overwash regime, in which waves overtop the dune and dune lowering and island roll-over may take place; (4) and the inundation regime, where the surge and wave set-up is sufficient to entirely inundate the barrier island and the island may become drowned. Although the Storm Impact Scale was originally derived for barrier islands, the concepts are valid for many natural sandy coasts. The simulated morphodynamic response of a barrier island to the four impact regimes, based on work by McCall et al. (2010), are shown in Fig. 11 for simulations with and without IG wave processes computed using the XBeach model (Roelvink et al., 2009). In the swash regime of this simulated barrier island, the model suggests that IG waves lead to greater beach erosion and a quicker transition to dune scarping (top left panel in Fig. 11), where the increase is determined by the relative contribution of IG waves to the nearshore wave energy. In the collision regime, the model suggests that IG waves allow for greater water depth, and thus more short-wave energy, at the base of the dune, and enhance the undertow in the surf zone, leading to a substantial increase in the computed eroded volume of the dune (cf. Van Thiel de Vries, 2009; Van Rijn, 2009, and top right panel in Fig. 11). The IG components in the swash, which are dominant on the dissipative beach of the simulated barrier island during high-energy events, are the key factor causing the transition from the swash regime to the collision regime, and from the collision regime to the overwash regime, and therefore strongly determine both the onset of dune scarping and overwash and lowering (cf. Cañizares and Irish, 2008 and centre panel in Fig. 11). In the inundation regime, steady flow driven by a pressure gradient across the simulated barrier island becomes the dominant sediment transport mechanism, and thereby reduces the relative contribution of IG waves to the post-storm bed profile (cf. Muller et al., 2016; McCall et al., 2010, and bottom panel in Fig. 11).

The numerical model investigations discussed in this section suggest that IG waves contribute strongly to the morphodynamic response of dissipative sandy coasts to a wide range of storm conditions, in particular in the collision and overwash regimes. Furthermore, they have the potential to change the type of morphodynamic response of the coast (e.g., overwash and flooding, instead of dune scarping) by steering the transition between these regimes.

4.2. Tidal inlets

Over the last decade, several studies relying on field measurements (Wargula et al., 2014; Orescanin et al., 2014) and/or numerical modelling (Bertin et al., 2009; Bruneau et al., 2011; Nahon et al., 2012; Dodet et al., 2013) have shown that short waves can have a relevant contribution in the hydro-sedimentary dynamics of tidal inlets through a large range of processes. Conversely, the relevance of IG waves in tidal inlets was only investigated very recently (Bertin and Olabarrieta, 2016; Williams and Stacey, 2016). The generation mechanisms and propagation of IG waves in tidal inlets might differ substantially from the beach environments due to the complex morphology of tidal inlets including locally very steep bottoms (e.g. terminal lobe of the ebb delta) and the presence of strong tidal currents in the main channels.

Williams and Stacey (2016) performed field measurements at the Pescadero Estuary Mouth, California, and identified fluctuations in water levels and current velocities in the IG band. These authors described the waves as bores propagating inside the lagoon that were larger when the offshore significant wave height increased. Williams and Stacey (2016) also showed that velocities associated with IG waves were of the same order of magnitude or even larger than tidal currents, although they rapidly decrease after the beginning of the ebb.

Bertin and Olabarrieta (2016) investigated the relevance of IG waves at Albufeira Lagoon Inlet, a shallow wave-dominated inlet located on the Western Coast of Portugal. Field measurements of water levels and currents carried out both inside and outside the lagoon under a moderate energy but long period swell revealed the occurrence of low-frequency fluctuations in the IG band. Outside the lagoon, these fluctuations were present along the whole tidal cycle, whereas inside the lagoon they disappeared a few hours after the beginning of the ebb tide until the next rising tide (Fig. 12). In addition, these authors im-

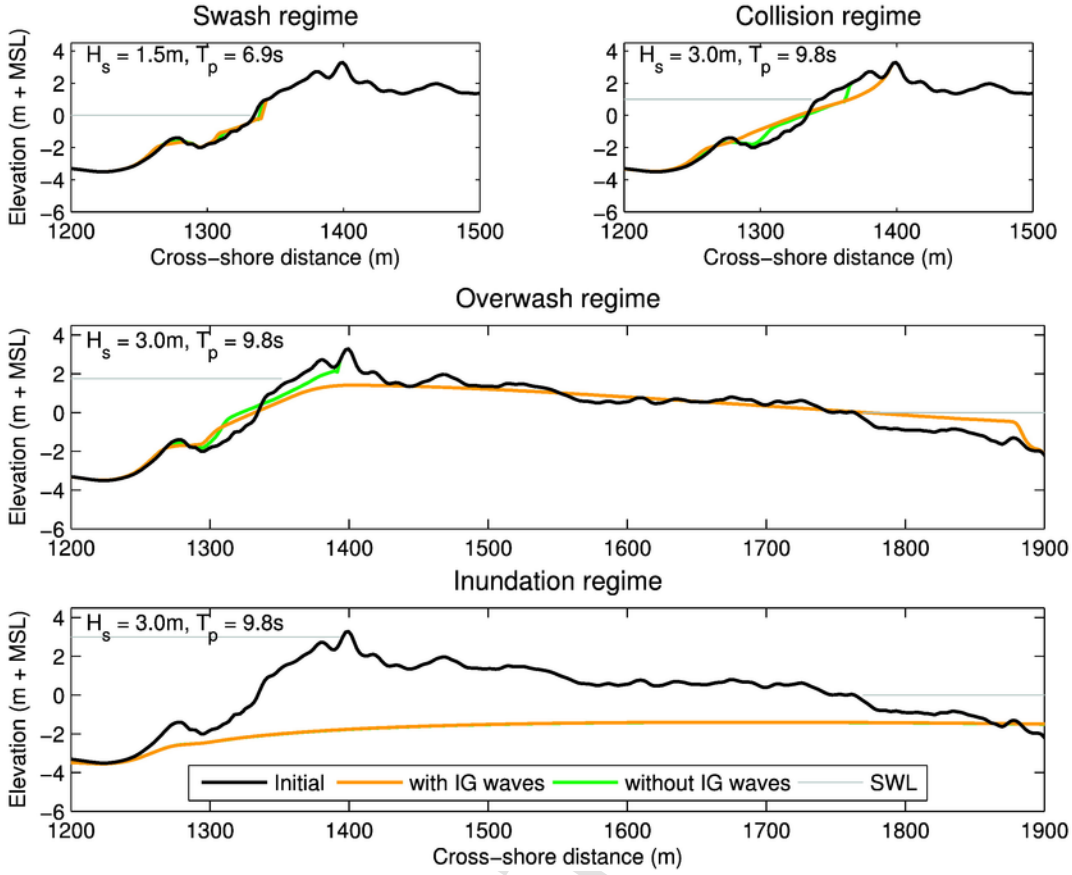

Fig. 11. Simulated morphological change of a cross-shore profile of a barrier island based on McCall et al. (2010) using the XBeach model with (orange) and without (green) IG waves. Four simulations are run in which the barrier island is exposed to four different water level, wave height and wave period forcing conditions for a duration of three hours to characterise storms in the swash, collision, overwash and inundation regimes, as defined by Sallenger (2000). Differences between the models are particularly apparent in the collision and overwash regime.

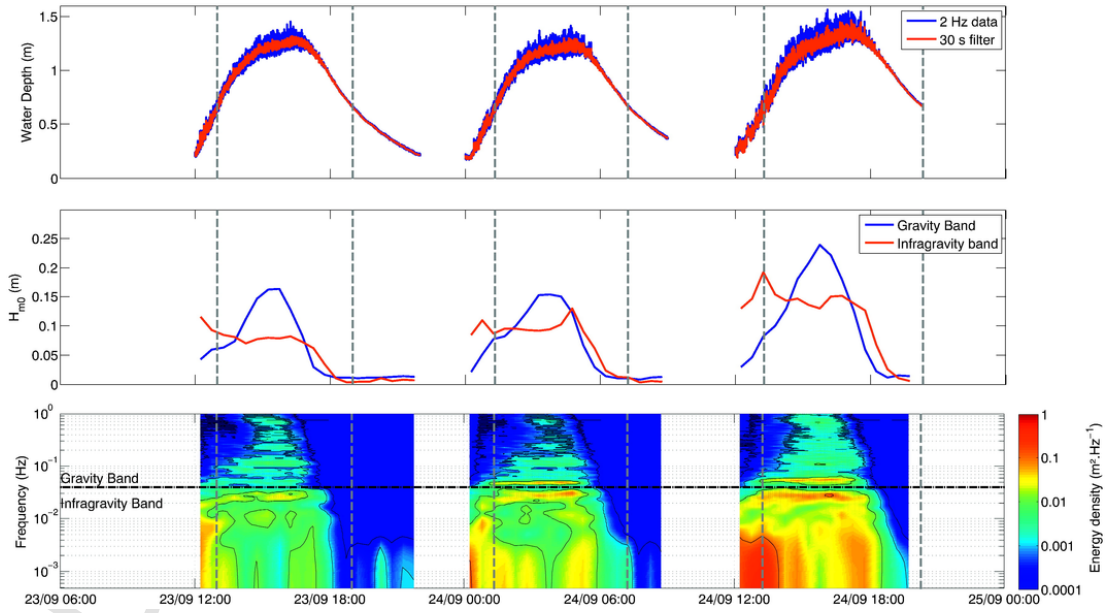

Fig. 12. Time-series of observed water depths (top), H_{m0} in the gravity (blue) and in the (red) IG bands (middle) and frequence repartition of the energy density inside the Albufeira Lagoon (Portugal) in September 2010.

plemented the XBeach modelling system (Roelvink et al., 2009) and reproduced fairly well the generation and propagation of IG waves, including the drop of their energy during a large part of the ebb. This behaviour was explained by blocking due to opposing tidal currents reaching 2.5 $m.s^{-1}$ in shallow water depths. Bertin and Olabarrieta (2016) also performed numerical experiments where they removed

wave forces inside and outside the surfzone, which showed that the breakpoint mechanism and the bound wave mechanisms both contributed significantly to the generation of IG waves in the inlet. Inside the lagoon, IG waves induced fluctuations in flood currents reaching temporarily 100 % of their magnitude. The fact that these fluctuations occur mostly at flood and not at ebb should promote flood dominance in the lagoon and might contribute to the shoaling and possibly the closure of such shallow inlets during winter storms.

These findings will have to be verified at other inlet systems under various incident wave conditions. In particular, these studies did not include sediment transport measurements and the possible contribution of IG waves in the closure of shallow systems will have to be investigated in detail. These studies showed that IG waves get blocked during the ebb due to strong counter currents in shallow depth. Such blocking could hardly occur in deeper inlets, except if ebb deltas are tilted and face the main channel so that strong counter currents can locally flow in shallow depths across the surfzone.

4.3. Reef hydrodynamics

4.3.1. Coral reefs

Many tropical islands and coasts are lined with coral reefs. These reefs not only host valuable ecosystems but also act as a flood defense to protect coastlines from coastal storm damage and flooding. Over reefs, incident-band (and predominantly remotely-generated swell) waves break in a narrow surf zone on the reef edge, where most of the waves are dissipated and little energy (typically 2% in the short-wave band, Ferrario et al. (2014)) is transmitted to shore. However, particularly during storm and large swell conditions, overwash and coastal flooding still occur due to high water levels (Jaffe and Richmond, 1992; Hoeke et al., 2013), overtopping due to both short waves, IG waves and/or low-frequency wave resonance (Merrifield et al., 2014; Cheriton et al., 2016). The mechanism behind this is radiation stress gradients associated with wave breaking that not only produces a well-known steady set-up which can be quite large on reefs (on the order of 1.0 m (Munk and Sargent, 1948; Vetter et al., 2010)), but also produces a time-varying component due the groupiness of the incoming waves, which causes the breakpoint to vary in time and space, as explained in Section 2.2. In the case of reefs, these breakpoint-generated IG waves (Symonds et al., 1982) usually dominate over IG waves generated through the bound-wave shoaling mechanism introduced in Section 2.1 (Battjes et al., 2004; Pomeroy et al., 2012; Merrifield et al., 2014). Nwogu and Demirbilek (2010) found, on the basis of laboratory experiments on an idealized smooth reef, that IG energy increased across the reef flat towards shore. In another laboratory study, Pomeroy et al. (2015) found that incident-band waves decreased rapidly at the reef crest, then more gradually across the flat. IG waves also shoaled and then rapidly decreased in height at the crest, but instead grew higher as they propagated across the reef flat.

As a result of the generation of IG waves on the reef edge, the wave spectra become bi-modal on the reef flat (Young, 1989; Hardy and Young, 1996). There, the remaining incident waves and to a lesser extent IG waves (Pomeroy et al., 2012)) attenuate due to bottom friction dissipation, which is larger than that typically found on sandy beaches (Lowe et al., 2005; Monismith et al., 2015). This implies that IG waves become more and more dominant away from the reef edge, as confirmed by numerical analysis by (Van Dongeren et al., 2013) for a wide fringing reef (Fig. 13). These authors showed that the influence of short waves decreases dramatically across the reef flat and within the lagoon, typically accounting for $< 40\%$ of the bed shear stresses, while the contribution of IG waves to the total bed shear stresses gradually increases across the reef towards the lagoon and ultimately turns dominant (generally accounting for up to 50% of the bed shear stress in the lagoon).

Using numerical simulations, Shimozono et al. (2015) showed that, for the case of a typhoon impact on a narrow reef-lined coast in the Philippines, the run-up spectrum was more dominated by IG waves if the reef was wider. The IG wave attenuation is controlled by wave shape, bed roughness, water depth, and the width of the reef flat (Péquignet et al., 2009). For large roughness, wide reefs and/or small water depths, IG waves are shoreward propagating with little reflection from the coastline. In contrast, for smooth reefs and for certain combinations of reef width, water depth and incident wave period, resonance may occur on the reef, with associated large sea surface amplitudes at the shoreline (Cheriton et al., 2016; Gawehn et al., 2016). Furthermore, IG waves that reflect from the shore may escape to deeper water, where they are hardly attenuated, and impact the opposite coast (Rawat et al., 2014). Few studies so far have included the alongshore variations in the reef topography, which may amplify wave heights or set-up(Smithers and Hoeke, 2014; Rogers et al., 2015). Beetham et al. (2016) suggested that the overprediction of the modelled IG waves may be the result of excluding longshore variations. All factors - set-up, resonance, IG waves and short waves - contribute to potential flooding of the coastline and damages on islands.

4.3.2. Rocky shore platforms

Over the last decade, a number of studies have observed IG wave characteristics on shore platforms, particularly in the meso- and micro-tidal environments of New Zealand and Australia (e.g. Beetham and Kench, 2011; Ogawa et al., 2015; Ogawa et al., 2011; Marshall and Stephenson, 2011), and their results have mostly agreed with those from coral reefs. Microtidal, rocky shore platforms, sometimes referred to as Type B platforms (Sunamura, 1992), provide a morphology that is analogous to coral reefs in that they are near-horizontal with a steep low-tide cliff, the upper part of which can sometimes be seen at low tide. Of these studies, the only one to focus entirely on IG waves is that of Beetham and Kench (2011) who observed the IG-wave height to be linearly dependant on the offshore short-wave height and to increase shoreward with a maximum IG wave height of 0.20 m measured at the cliff toe. Ogawa et al. (2015) showed that the importance of IG waves on a shore platform can be parameterized using the relative water depth (h/H) at the platform edge. A threshold value of 1.1 was observed, above which sea-swell frequencies dominate the wave spectra, and below which IG frequencies dominate the wave spectra as short waves typically break on the platform edge.

4.4. Seiches in semi-enclosed basins and harbours

Semi-enclosed basins and harbors have natural resonant periods ranging from a few tens of seconds to a few hours. The amplitude of small oscillations coming from the ocean may be strongly increased by resonant processes (Rabinovich, 2009). This phenomenon is known as coastal seiches (Giese and Chapman, 1993; Rabinovich, 2009) and creates important hazards for population safety and economic activities. Harbors are particularly vulnerable to these phenomena, which can seriously affect operations and cause severe and expensive damages to harbor facilities and moored ships. Associated currents can also drive substantial sediment transport and may modify the harbor bathymetry. These problems have fostered numerous studies aimed to better understand the development of such seiches in harbours (De Jong and Battjes, 2004; Lee, 1971; Okihiro et al., 1993, among others).

The long waves responsible for seiche development may be generated by a large range of mechanisms, including seismic phenomenon, internal waves and jet-like currents. However, the most common mechanisms driving coastal seiches in harbours are related to atmospheric disturbances (Vilibić et al., 2008) and IG waves (Ardhuin et al., 2010). For small-scale basins with resonant periods of a few minutes, Okihiro et al. (1993) showed that seiches are forced mainly by IG waves.

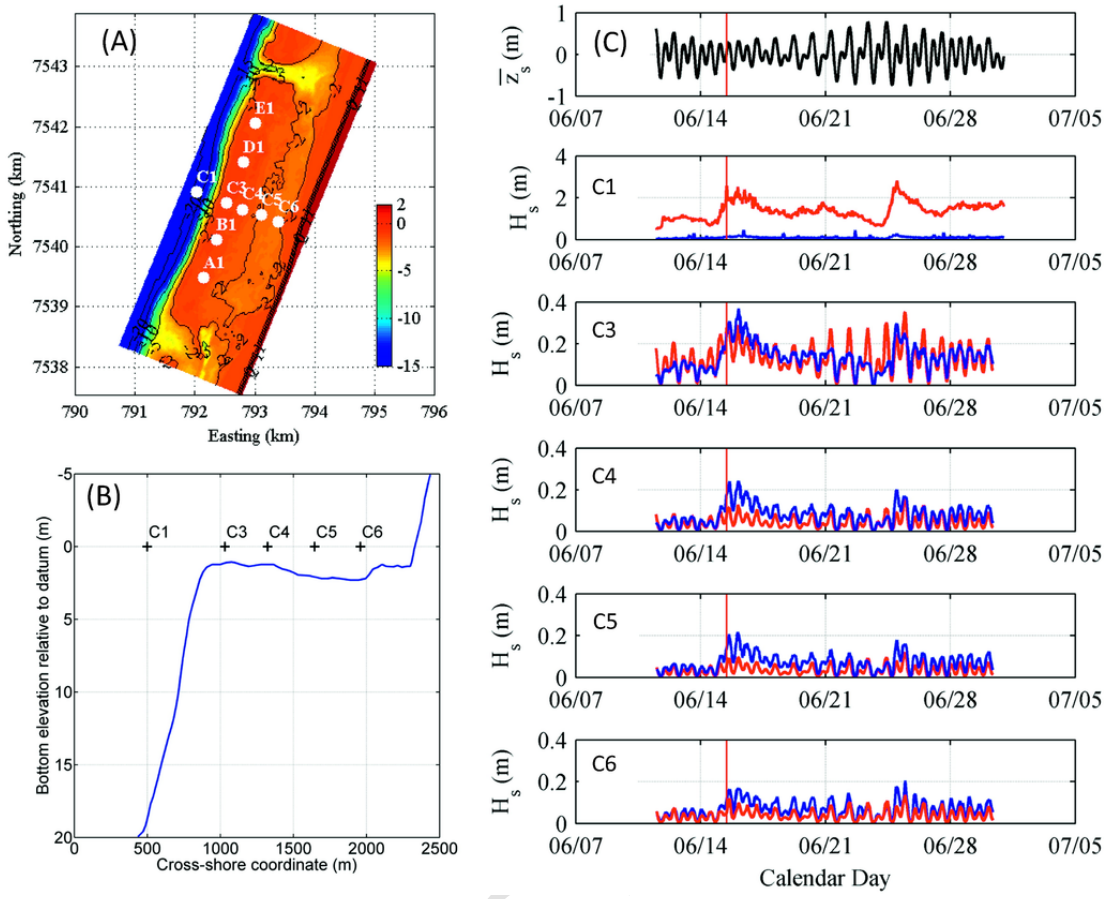

Fig. 13. (A) Bathymetry of Ningaloo Reef (Western Australia) and location of the sensors, (B) cross-shore profile of the reef at the location of the sensors and (C) Time series of the mean water level (tide) measured on the forereef at C1 and Root-mean-square wave heights for the IG wave band $H_{rms,IG}$ (blue) and short-wave band $H_{rms,sw}$ (red) measured across at C1, C3, C4, C5 and C6). Modified from Van Dongeren et al. (2013).

In order to illustrate this phenomenon, we focus here on the case study of Port-Tudy harbour, located on Groix Island on the Western Coast of France (see Fig. 14a). Strong seiches regularly develop in this harbour, with some of the highest amplitudes observed along the French metropolitan coast.

4.4.1. The resonant periods

The resonant periods, also known as eigen periods, of semi-enclosed basins (such as gulfs, bays, fjords, inlets, ports, or harbours) are fully determined by the basin geometry. In order to characterize the resonant periods of Port-Tudy harbour, the background spectrum is computed on the water surface elevations time-series observed during the calm periods of the year 2013. Calm periods were arbitrarily defined as periods of more than 4 consecutive days where the significant height of low-frequency oscillations in the harbour was lower than 0.15 m. The resulting background spectrum (see Fig. 14b) clearly shows a unique broadened peak, with a peak period centred around 5 min and extending from 3 to 6 min. The broadened peak is explained by large tidal level variations, which can reach about 5 m during spring tides in this area. As wave propagation depends on the water depth, the resonant period varies during the tidal cycle, resulting in the observed broadened peak.

However, resonance implies the development of standing waves so that the elevation signal measured at a fixed tide gauge, potentially close to an oscillation node, may not be representative of the whole harbour. To overcome this problem, the tide gauge analysis was complemented with a numerical model solving the Berkhoff (1972) equations to compute the eigen modes of oscillations inside the harbour. Model results revealed resonant periods ranging from 3.08 min for the highest astronomical tide to 5.95 min for the lowest astronomical tide, which is consistent with the observed background spectrum (Fig. 14b).

4.4.2. Forcing mechanisms

The seiche magnitude, H_{Seiche}, is estimated at the tide gauge location, as the significant wave height computed over periods ranging from 3 to 6 min. The time series of observed H_{Seiche} is plotted (black line) in Fig. 14c for the whole year 2013 and first month of 2014. During this period, the maximum observed H_{Seiche} reaches 1.1 m on 6 January 2014.

In order to explain the development of these seiches, the significant height of the incoming bound waves $H_{Hasselmann}$ was computed according to Hasselmann (1962) from time series of directional spectra computed offshore of Groix Island Fig. 14a from an application of the WWIII model for the French Coasts (Ardhuin and Roland, 2013) . Fig. 14c shows a strong correlation between the observed seiche height in the harbour and the modelled incoming bound wave, with a Pearson correlation coefficient reaching 0.85 for the considered period. Based on this correlation, together with results presented above, we propose that the development of seiches in the harbour results from the amplification by resonance of IG waves, released around the island and trapped inside the harbour. This hypothesis will be verified in the future using process-based models capable of simulating coastal IG waves (e.g. Roelvink et al., 2009).

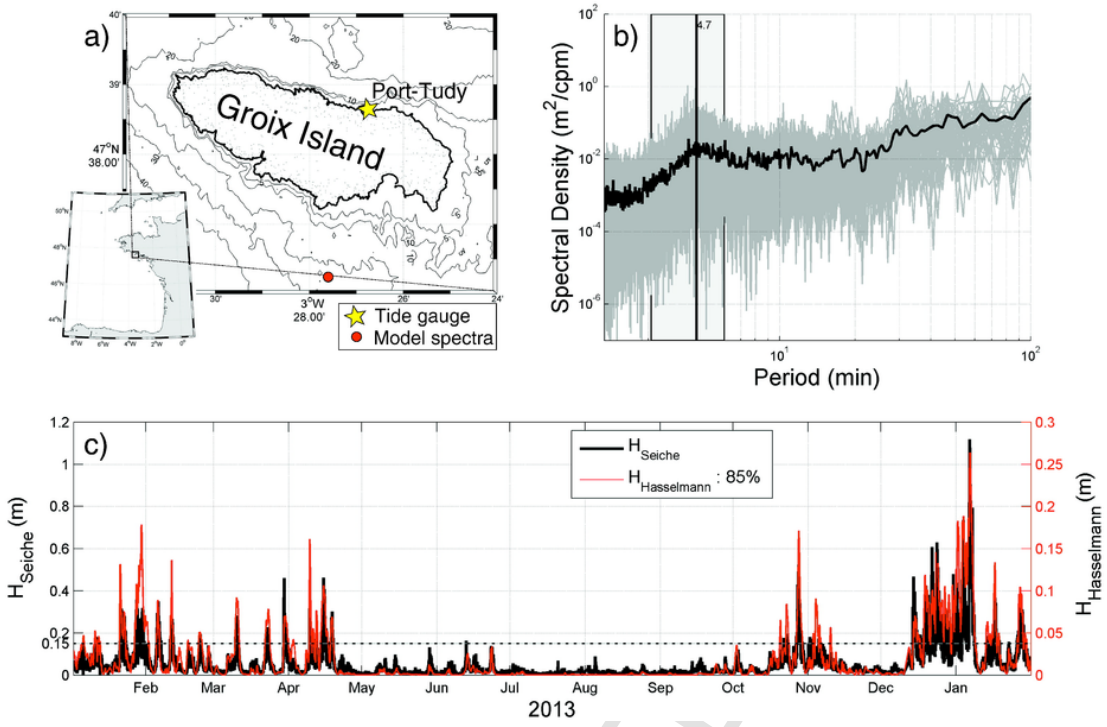

Fig. 14. a) Location and bathymetric map of Groix Island and Port-Tudy. b) Background spectra (grey lines) and mean background spectrum (black line) computed on time series (calm periods) recorded with Port-Tudy tide gauge. The grey box represents the range of eigen periods obtained with the model. c) Significant height of seiche (H_{Seiche}) and IG waves ($H_{\text{Hasselmann}}$) time-series during the whole year 2013 and the first month of 2014.

4.5. Free IG waves and associated seismic waves in the solid Earth: the hum

4.5.1. Properties of the hum

Nawa et al. (1998) discovered ground oscillations at land seismic stations with periods longer than 30 s but which are not caused by earthquakes. This unexpected background signal varies stochastically on the short term but has two yearly maxima (Tanimoto, 2005) that correspond to the storm seasons of each hemisphere. The propagation direction of these seismic waves clearly associates this "hum" from 30 to 300 s with ocean waves (Rhie and Romanowicz, 2004; Bromirski, 2009; Nishida, 2013). At 300 s, the seismic wavelength is on the order of 1500 km. These waves are long enough that their interference around the planet excites the Earth's normal modes, frequencies separated by approximately 10^{-4} Hz at which the Earth rings like a bell. The ' tone' of these oscillations can be used to infer properties of the solid Earth.

Whereas shorter microseisms, with periods under 30~s, are now relatively well understood, a quantitatively verified theory of the hum generation by free IG waves is very recent (Ardhuin et al., 2015), and many alternative theories have been proposed by Tanimoto (2005); Webb (2007, 2008); Uchiyama and McWilliams (2008); Traer and Gerstoft (2014), among others. In general, all these authors have linked oceanic IG waves with the hum. A better understanding of the generation of the hum could thus offer a possible way to measure IG waves from land-based seismometers, and help refine the use of microseism background signals to investigate the structure of the Earth.

A Fourier analysis of motions in the solid Earth and ocean layer shows that the transfer of energy from ocean waves to seismic waves is significant only if ocean wave motions match both the wavelength and periods, and hence the speed, of seismic waves (Hasselmann, 1963). This necessary matching of the speeds of different wave trains applies to all sorts of wave motions (Hasselmann, 1966), for example the generation of atmospheric waves by tsunamis (e.g. Artru et al., 2005). Two types of interactions can be the match-makers between IG waves, which travel at a few hundreds of metres per second, and much faster seismic waves, which reach 5 km/s at the seafloor. The primary mechanism is an interference of surface waves of wavenumber $\mathbf{k}_w$ and frequency f_w with bottom topography $\mathbf{k}_b$, which produce seismic waves of wavenumber $\mathbf{k}_s = \mathbf{k}_w + \mathbf{k}_b$ and frequency $f_s = f_w$. The secondary mechanism is the interference of two wave trains of wavenumber and frequency $(\mathbf{k}_1,f_1)$, $(\mathbf{k}_2,f_2)$, producing a seismic wave of wavenumber $\mathbf{k}_s = \mathbf{k}_1 + \mathbf{k}_2$ and frequency $f_s = f_1 \pm f_2$. Because $|\mathbf{k}_s|/(2\pi f_s)$ must be equal to the seismic phase speed, these resonance conditions impose $\mathbf{k}_2 \simeq -\mathbf{k}_1$ and thus $f_1 \simeq f_2$ and $f_s \simeq 2f_1$. These conditions make it impossible for the interaction $f_s = f_1 - f_2$ to produce a significant seismic wave amplitude (Hasselmann, 1963; Webb, 2008), contrary to the propositions by Uchiyama and McWilliams (2008) and Traer and Gerstoft (2014).

Without any of these two mechanisms, ocean waves propagating over a flat bottom only produce pressure oscillations in the water and a deformation of the bottom that is proportional to the local ocean wave amplitude but which cannot propagate as seismic waves. This effect is known as compliance and is used in geophysical studies of oceanic crustal structure (e.g. Crawford et al., 1991). Ardhuin et al. (2015) applied the wave-wave and wave-bottom interaction theories of Hasselmann (1963), taking into account the necessary correction for finite depth given by Ardhuin and Herbers (2013). The result is shown in Fig. 15. The secondary mechanism is too weak by 10 orders of magnitude to explain the recorded hum, whereas a reasonable guess of an effective bottom slope of 6%, combined with the global IG wave model of Ardhuin et al. (2014) gives a good agreement between both the mean observed hum level (Fig. 15) and its temporal variability (Ardhuin et al., 2015).

4.5.2. Free IG waves in the open ocean

Assuming uniform topography along-shore, Ardhuin et al. (2015) showed that the interference of waves and bottom topography is domi-

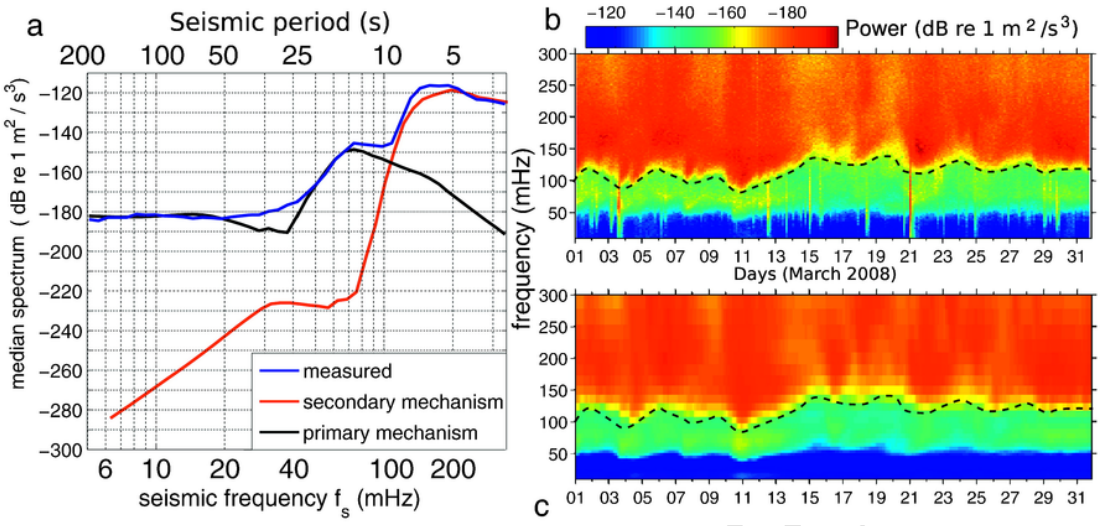

Fig. 15. Measured and modelled seismic spectra. (a) Vertical acceleration power spectral density (PSD) in March 2008 at the French SSB seismic station, located near Saint-Etienne, France. (b) Observed and (c) modelled PSDs in March 2008 following Hasselmann (1963) and Ardhuin et al. (2015). Light blue to red vertical stripes correspond to earthquakes (not modelled). The dashed line separates the low frequencies where the primary mechanism dominates from the higher frequencies explained by the secondary or 'double-frequency' mechanism. The Johanna storm, on March 10, is conspicuous with powerful and lower frequency microseisms.

nated by what happens around the non-dimensional depth $kD = 0.76$ (wave numbers time water depth). For periods 50 to 300~s, hum sources are therefore expected to be at depths of 300–1000 m, corresponding to the position of the shelf slope. Although the magnitude of the hum source depends on the generally poorly constrained effective slope, the relative variation of hum amplitudes could provide a useful complement to the few available measurements of open ocean IG wave measurements. Very few data were available in the open ocean 25 years ago (Webb et al., 1991), but a few real-time seafloor data series are now available from the Neptune network off the coast of British Columbia and more and more bottom pressure recorders are being deployed for marine geophysics experiments (Davy et al., 2014; Godin et al., 2014) and the tsunami warning system (e.g. Aucan and Ardhuin, 2013). A better knowledge of sources and propagation patterns of IG waves across oceans is thus emerging. The global IG wave field combines strong sources on west coasts that radiate towards the east (Rawat et al., 2014), with some occasional free waves arriving from the open ocean (Neale et al., 2015). Mid-ocean observations in the North Atlantic by Crawford et al. (2015) suggest that summer IG events can have significant sources in the southern hemisphere. Although some details are still unclear, these features are generally consistent with a global model fed by empirical sources of free IG waves at the coast giving average IG wave heights shown in Fig. 16.

Given the large scale extension of free IG sources along the coast, it seems unlikely that hum or open ocean IG wave recordings will provide detailed information about the IG wave generation processes. Nevertheless, these measurements provide a general constraint on the IG energy balance and regional averaged levels of free IG waves generated at the coast.

5. Conclusions and future challenges

5.1. Future challenges for knowledge improvement

Over the past few decades, IG waves have received considerable attention from the coastal community, which has led to important progress in understanding their generation mechanisms, transformations and impacts in the nearshore. Despite these advances, numerous questions remain to be explored, and new challenges have also emerged. In addition to challenges listed at the end of each subsection above, we summarize below the most relevant ones (in our opinion) for the coastal scientific community.

Regarding IG wave generation mechanisms, the importance of the phase lag between the long bound wave and the wave energy envelope should receive more attention. Even though this phenomenon was observed several times in the field (e.g. Masselink, 1995; Inch et al., 2017a), its detailed analysis is restricted to a few lab experiments (e.g. Janssen et al., 2003). In particular, its dependence on the incident wave spectra as well as the beach slope should be further investigated. The understanding of the breakpoint mechanism should also be improved, through new field measurements collected over steep bottoms, which are scarce in the literature. Also, the relationship between the frequency of IG waves and the shape of the incident short wave spectra is not totally understood, as both relatively short period IG waves (e.g. $T < 60s$) were observed under narrow banded long period incident waves (e.g. Bertin and Olabarrieta, 2016) and larger period IG waves were observed under shorter period incident short-waves (e.g. De Bakker et al., 2014). Such field measurements could be complemented with numerical modelling using surf beat models, where wave forces can be turned off outside and inside the surfzone to analyse the respective contribution of these mechanisms. Furthermore, the transfers of IG wave energy back to short waves and the generation of IG harmonics and subsequent depth limited breaking needs to be studied for more types of coasts (e.g. gravel beaches, rocky shores, tidal inlets and estuaries and coral reefs). In particular, the respective contribution of both mechanisms to the observed IG wave energy loss in the nearshore should be better quantified. In order to better understand the fate of IG waves in the very nearshore, intercomparisons of separation techniques should be promoted, namely to better evaluate the uncertainty associated with reflection coefficient estimates (e.g. Inch et al., 2017b). Measurements of the free surface elevation with photogrammetry (e.g. de Vries et al., 2011) or LiDAR scanners (Martins et al., 2017) techniques combined with the Radon separation technique (Almar et al., 2013) appear to be a promising perspective.

The review of the studies about the impact of IG waves on sediment transport revealed contrasting observations. The ratio of IG wave height to short wave height (highly dependent on beach slope and offshore wave conditions) was shown at several sites to explain the type of sand suspension mechanism and thereby subsequent sand transport magnitude and direction. This hypothesis needs to be verified for vari-

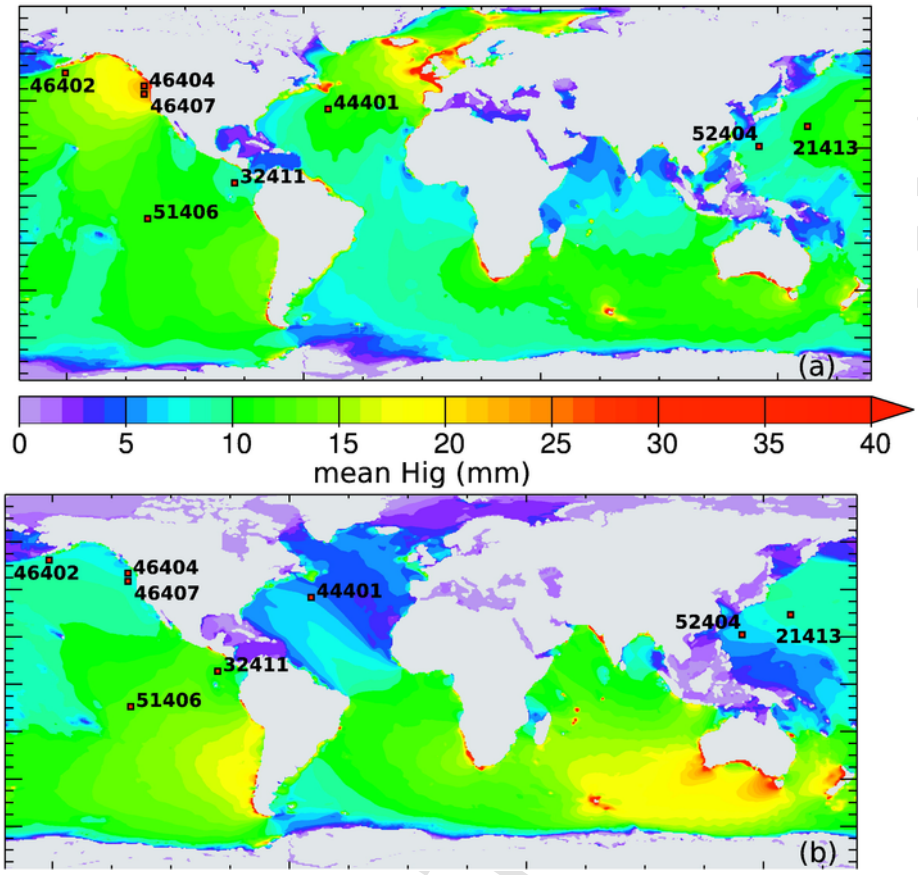

Fig. 16. Mean values of H_{IG} over (a) January and February 2008, (b) June and July 2008. Small square with numbers correspond to the location of DART stations used here for model validation. Taken from Ardhuin et al. (2014).

ous beach morphologies and under a wide range of incident wave conditions. In particular, high-resolution measurements under high energy conditions are particularly needed, along transects spanning from the shoaling zone (with structures deployed offshore and combining pressure/velocity sensors), to well within the swash zone. In addition, for a given site and level of IG wave energy, the magnitude of the associated currents and subsequent sand fluxes should be strongly impacted by the period of IG waves. This hypothesis should be verified in the field, measuring sand fluxes under IG waves of similar energy but with different periods. These improvements would also benefit process-based morphodynamic models (e.g. XBeach, Roelvink et al., 2009), which use parameterized approaches for sand fluxes with little validation under extreme events.

5.2. Broader implications

The further improvement of knowledge on IG-wave dynamics will also benefit other scientific communities. As mentioned briefly in the Introduction, recent studies point out the important role of IG waves at the various sea-interfaces: the generation of acoustic waves in the thermosphere, the creation of the earth's hum at the seafloor, as well as their influence on ice-shelf collapse. In addition, for the field of sedimentology specific to coastline evolution, the IG erosional/depositional imprints are expected to be considerable. Furthermore, the IG wave impacts, especially during storms, need to be taken into account when providing operational forecasts, and when assessing longer-term coastline stability. IG waves should also be considered during harbour design, as they can effect harbour operations substantially through resonance.

Acknowledgements

The review paper was fostered during a workshop on IG waves organized in La Rochelle (France) on the 17–18th March 2016, which was sponsored by Région Poitou-Charentes, the Charente-Maritime Council and the municipality communities of La Rochelle. XB, TG and ADB were funded by the Chaire Regional Program EVEX and ADB received in addition to a PRESTIGE incoming mobility grant, co-financed by the FP7 Marie Curie Actions-COFUND (grant agreement no PCOFUND-GA-2013-609102). G.D. was funded by the research program PROTEVS (12CR6) conducted by the French Naval Oceanographic and Hydrographic Department (SHOM). GR was funded by the Dutch Technology Foundation STW (Vici project 13709).

Appendix A. Separation methods

As the incoming infragravity wave can (partly) reflect from the beach and travel offshore, the sea-surface elevation timeseries η is a superposition of both the incoming and outgoing infragravity wave. To determine the amount of reflection of the incoming infragravity-wave energy, and to study the incoming infragravity-wave transformation, one needs to separate the two signals. Several techniques have been developed to separate the incoming from the outgoing infragravity wave, varying from a time-domain method (Guza et al., 1984) and two spectral-domain (Sheremet et al., 2002; Van Dongeren et al., 2007) methods, based on the Fourier transform of the wave-field, to the Radon Transform for two-dimensional wave fields (Radon, 1917; Almar et al., 2013, 2014).

The first three methods assume normally incident waves on flat beds, but as both assumptions are usually violated in shallow coastal waters this might introduce considerable errors. Sheremet et al. (2002) have investigated the effect of these assumptions on their method and concluded that the relative errors of both energy fluxes and reflection coefficients for their field data do not exceed 20%. A comparison between Sheremet et al. (2002)s method and the array method of Van Dongeren et al. (2007) shows that at the low end of the infragravity frequency band, which is characterised by long wavelengths, reflection estimates are highly effected by the number of consecutive sensors (De Bakker et al., 2014). In addition, reflection coefficients from 'noisy' field data may be biased high (Tatavarti et al., 1988; Huntley et al., 1999; Inch et al., 2017b).

A.1. PUV methods

A.1.1. Time-domain approach by Guza et al 1984

The time-domain approach developed by Guza et al. (1984) uses co-located wave gauges and velocity meters to construct surface elevation time series of the incoming η^+ and outgoing η^- signals,

$$\eta^{\pm} = \frac{\eta \pm \left(\frac{h}{g}\right)^{1/2} u}{2}, \tag{9}$$

where h is water depth and g is gravitational acceleration.

A.1.2. Spectral-domain method by Sheremet et al. 2002

The spectral-domain method of Sheremet et al. (2002) also uses co-located wave gauges and velocity meters, but has incoming and outgoing energy fluxes $F_f^{\pm}$ as output for separate frequencies following,

$$F_f^{\pm} = N_f^{\pm}\sqrt{gh}, \tag{10}$$

$$N_f^{\pm} = \frac{1}{4}\left[C_{\eta\eta,f} + \frac{h}{g}C_{uu,f} \pm \left(2\sqrt{\frac{h}{g}}\right) C_{\eta u,f}\right], \tag{11}$$

where N is the energy, $C_{\eta u}$ is the $\eta - u$ co-spectrum and $C_{\eta\eta}$ and C_{uu} are η and u auto-spectra, respectively. Summation over infragravity frequencies gives the bulk infragravity energy flux, $F_b^{\pm}$. The bulk reflection coefficient, R_b^2, is defined as the ratio of the offshore to onshore propagating bulk infragravity energy flux, $R_b^2 = F_b^-/F_b^+$.

A.2. Array methods

Array methods decompose a wave signal into its shoreward and seaward propagating components by using a cross-shore array of spatially separated pressure sensors only (i.e., without velocity data) and rely on the phase difference of waves between individual sensors. Array methods provide an estimate of the incident and reflected infragravity components at the centre of the instrument array used in the analysis. A number of these methods exist, operating in both the time (e.g. Frigaard and Brorsen, 1995) and frequency (e.g. Goda and Suzuki, 1976; Mansard and Funke, 1980; Van Dongeren et al., 2007) domains. Pressure sensors are typically more economical than velocity sensors allowing a wider range of spatial measurements with lower cost, thus obtaining a better appreciation of the spatial variability in infragravity wave dynamics. Furthermore, pressure sensors less obtrusive and more robust so can be deployed for longer time periods, essential when investigating the climatology of infragravity waves.

Most array methods are intended for the study of two dimensional waves propagating over a horizontal bed and are not designed for use on a sloping, natural beach. Baldock and Simmonds (1999), using the method of Frigaard and Brorsen (1995), showed that ignoring the effects of wave shoaling can lead to errors of up to 90% in the estimation on incident and reflected wave amplitudes. However, they also demonstrate that relatively simple modifications are needed to adapt array separation methods for using on sloping beds. Indeed, the method of Van Dongeren et al. (2007) is adapted from that of Battjes et al. (2004) with modifications for shoaling and phase speed effects.

An important consideration in the study of infragravity waves is that array methods require a strategic approach to the separation distance between pressure sensors to avoid singularities occurring at discrete frequencies where the sensor spacing is typically equal to an integer number of half wavelengths. For this reason, array methods perform best with three or more pressure sensors spaced unevenly to provide a greater range of separation distances for use in the analysis. Although, as more pressure sensors are used, the subsequent wave reflection estimates are averaged over a larger cross-shore range.

A study by Inch et al. (2017b) showed that an additional source of error that can affect array methods, particularly in the field, is random signal noise. Using numerical simulations, they show that the presence of noise introduces a significant positive bias to incident and reflected spectra estimates, and corresponding reflection coefficients. A technique is introduced that can be applied to any array method to investigate the impact of noise and develop a correction function for such noise. Applying this technique to the array method of Gaillard et al. (1980), a correction function is developed that, when applied to field data from a dissipative beach, suggests that infragravity reflection coefficients may be overestimated by as much as 50% because of noise.

A.3. Radon transform

A fourth method is the recently revisited Radon transform (Almar et al., 2013, 2014). So far it has only been tested on synthetic cases and laboratory data, but it shows good potential. It projects the two-dimensional wave field into polar space following,

$$R(\rho,\theta) = \oiint \eta(x,y)\; d(xcos\theta + ysin\theta - \rho)\; dx\; dy \tag{12}$$

where δ is the Dirac delta function, θ and ρ are the angle and distance from origin of the integration line defined as $\rho = xcos\theta + ysin\theta$. The origin is the center of the two-dimensional (x,t) wave field. Wave crests are identified as density peaks in the polar space. The wave field can be decomposed over the whole $x - t$ wave field as the incoming and outgoing wave trains appear in the Radon space within the $\theta = [1° - 89°]$ and $\theta = [91° - 179°]$ intervals, respectively. The original wave field can then be back projected with the Inverse Radon Transform applied separately to the different angles as,

$$\eta^+(x,t) = \int_{-\infty}^{+\infty}\int_{1}^{89} R(\rho,\theta)\; d\theta\; d\rho \tag{13}$$

$$\eta^-(x,t) = \int_{-\infty}^{+\infty}\int_{91}^{179} R(\rho,\theta)\; d\theta\; d\rho \tag{14}$$

The method seems relatively insensitive to wave characteristics, but is prone to the sampling scheme and the number and density of wave gauges. (The distance between gauges should be less than one third of the shortest wavelength, while the array should cover more than one third of the longest wavelength (Almar et al., 2014).)

Appendix B. Bispectra

Since the introduction of bispectral analysis by Hasselmann et al. (1963), it has been used in numerous studies to investigate nonlinearities of wave fields (e.g. Freilich and Guza, 1984; Elgar and Guza, 1985; Herbers et al., 1994, 1995; Norheim et al., 1998; Herbers et al., 2000; Thomson et al., 2006; De Bakker et al., 2015a,b). In addition to the power spectrum, which contains no phase information, the bispectrum B_{f_1,f_2} detects phase-coupling between frequency components, more specifically three frequencies. These triad interactions are responsible for the transfer of energy (pressure force times velocity) from the power spectral peak to sub- and superharmonics, which lead to a change in waveshape to skewed and asymmetric close to shore (e.g. Elgar and Guza, 1985). These energy transfers occur gradually to adjust to the decrease in water depth, and are stronger when water depths are shallower as waves are closer to resonance. The discrete bispectrum is defined as,

$$B_{f_1,f_2} = E\left[A_{f_1} A_{f_2} A^*_{f_1+f_2}\right], \tag{15}$$

where $E[\ ]$ is the ensemble average of the triple product of complex Fourier coefficients A at the frequencies f_1, f_2 and their sum $f_1 + f_2$, and the asterisk indicates complex conjugation. Similarly, the power spectrum is defined as,

$$P_{f_1} = \frac{1}{2} E\left[A_{f_1} A^*_{f_1}\right]. \tag{16}$$

The variance of the bispectral estimates is dependent on the power spectral properties of the signal, if not enough averaging is performed (by using blocks and frequency merging), the bispectral estimates might appear large just because it is highly variable. A normalized measure of the strength of the coupling of the interacting wave components, which removes this variance, the bicoherence $b^2_{f_1,f_2}$, is here defined as,

$$b^2_{f_1,f_2} = \frac{\left|B_{f_1,f_2}\right|^2}{P_{f_1} P_{f_2} P_{f_1+f_2}}, \tag{17}$$

following Collis et al. (1998), Eq. [27], and is the most commonly used normalization method for statistical tests, although it contains no upper bound. Several other ways exist in which bicoherence can be quantified, see for instance Haubrich (1965) and Kim and Powers (1979), the latter method having an upper bound of 1, when there is not averaged over frequency. For a comparison between the normalization methods, see for example Elgar and Guza (1988) and Collis et al. (1998). The 95% significance level on zero bicoherence is defined as 6/d.o.f., where d.o.f. is the degrees of freedom.

The normalized phase of the bispectrum, called the biphase β_{f_1,f_2} gives a normalized measure of the phase relationship and is defined as,

$$\beta_{f_1,f_2} = \arctan\left[\frac{\mathcal{I}\left\{B_{f_1,f_2}\right\}}{\mathcal{R}\left\{B_{f_1,f_2}\right\}}\right], \tag{18}$$

following Kim and Powers (1979), where $\mathcal{I}$ and $\mathcal{R}$ are the imaginary and real part of the bispectrum, respectively. The stability of the biphase estimates is highly dependent on bicoherence values; for low bicoherence, the biphase is randomly distributed between π and $-\pi$. The biphase can be related to the wave shape, with values close to zero (imaginary part is close to zero) indicating a skewed wave, and values close to -90 (real part is close to zero) indicating an asymmetric (e.g. Elgar and Guza, 1985). The biphase can be integrated over separate frequency bands, to single out the wave shape of the bound infragravity wave (biphase ≈ 180°) (e.g. De Bakker et al., 2015a).

As the bispectrum has symmetrical properties, it is only necessary to evaluate the bispectrum in the principal domain where $f_1, f_2 > 0$, $f_2 < f_1$ and $f_1 + f_2 < f_N/2$, where f_N is the Nyquist frequency (see for example Herbers et al. (2003)). The bispectrum is zero if the three frequencies are independent of each other, with random phase relationships in a linear wave field.

The imaginary part of the bispectrum shows relative energy transfers between the phase-coupled frequencies. Fig. 17 shows an example of a bispectrum in the outer surf zone obtained over a low sloping laboratory beach with a rather narrow banded spectrum. Positive (red) values at B_{f_1,f_2} indicate a transfer from f_1 and f_2 to f_3, the sum frequency. Negative (blue) values indicate a transfer from f_3 to f_1 and f_2. A positive interaction is present at B(0.44,0.44) where energy is transferred from the spectral peak to its higher harmonic at $f = 0.88$ Hz. Another positive, less strong interaction, is present at B(0.88,0.44) where energy is transferred from the spectral peak and its first harmonic to the second harmonic at $f = 1.32$ Hz. At the same time, negative interactions are present at B(0.42,0.04) with energy transfers from $f_3 = 0.46$ Hz to both $f_1 = 0.42$ Hz and $f_2 = 0.04$ Hz, and at B(0.86,0.04) with energy transfers from $f_3 = 0.90$ Hz to both $f_1 = 0.86$ Hz and $f_2 = 0.04$ Hz. These two interactions are responsible for the growth of the bound infragravity wave, while at the same time causing the energy around the spectral peak and its harmonics to shift to slightly lower frequencies, see also De Bakker et al. (2015a).

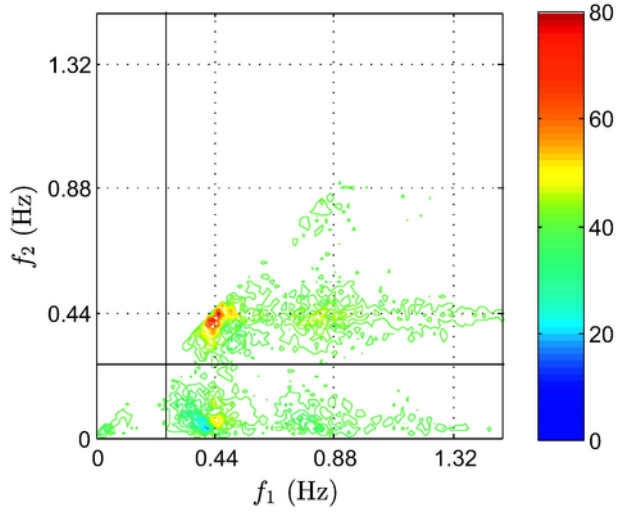

Fig. 17. Imaginary part of the bispectrum in m^3 (x 10^{-8}) of the incoming wave signal (η^+) over a 1:80 laboratory slope, at $x = 70$ m, $h = 0.18$ m. Black solid lines indicate

the cutoff between infragravity and sea-swell wave frequencies, f_{IG}. Dashed lines indicate the spectral peak (f = 0.44 Hz) and its higher harmonics. After De Bakker et al. (2015a).

By integrating over the imaginary part of the bispectrum and hereby combining all the separate interactions, and multiplying that with a coupling coefficient, net nonlinear energy transfers between frequencies S_{nl} can be calculated (e.g. Herbers et al., 2000; De Bakker et al., 2015a). The currently defined coupling coefficients vary from the Boussinesq scaling (e.g. Herbers and Burton, 1997) valid for resonant waves in shallow water, up to the more generalized theory (e.g. Janssen, 2006), which includes full linear dispersive effects. In shallow water during both shoaling and breaking sea-swell-wave conditions, the Boussinesq approximation yields the most reliable results (Herbers and Burton, 1997; Herbers et al., 2000; Smit et al., 2014), although the strong nonlinearities occurring in the surf zone are somewhat unrepresented, and third- and higher-order interactions would need to be incorporated for more reliable estimates (Thomson et al., 2006; De Bakker et al., 2015a). Using the stochastic formulation of the second-order nonlinear wave interaction theory of Herbers et al. (2000) (their Eq. (4)) S_{nl} can be determined discretely by:

$$S_{nl,f} = \frac{3\pi f}{h}\mathcal{J}\left\{\left(\sum_{f'=0}^{f}\Delta f\, B_{f',f-f'}\, - 2\sum_{f'=0}^{f_N-f}\Delta f\, B_{f',f}\right)\right\}. \quad (19)$$

The term $\sum_{f'=0}^{f} B_{f',f-f'}$ accounts for the sum interactions in the imaginary part of the bispectrum, and the term $-2\sum_{f'=0}^{\infty} B_{f',f}$ accounts for the difference interactions, as each particular frequency can participate simultaneously in both difference and sum interactions. To study interactions including infragravity frequencies in more detail, the bispectrum can be further divided into zones with different contributions of infragravity frequencies, after which S_{nl} can be determined for those separate zones (De Bakker et al., 2015a).

References

Aagaard, T., Greenwood, B., 1994. Suspended sediment transport and the role of infragravity waves in a barred surf zone. Mar. Geol. 118, 23–48.

Aagaard, T., Greenwood, B., 1995. Longshore and cross-shore suspended sediment transport at far infragravity frequencies in a barred environment. Cont. Shelf Res. 15, 1235–1249.

Aagaard, T., Greenwood, B., 2008. Infragravity wave contribution to surf zone sediment transport - the role of advection. Mar. Geol. 251, 1–14.

Aagaard, T., Greenwood, B., Hughes, M., 2013. Sediment transport on dissipative, intermediate and reflective beaches. Earth Sci. Rev. 124, 32–50. https://doi.org/10.1016/j.earscirev.2013.05.002.

Abdelrahman, S.M., Thornton, E.B., 1987. Changes in the short wave amplitude and wavenumber due to the presence of infragravity waves. In: Proc. of Specialty Conference on Coastal Hydrodynamics. American Society of Civil Engineers, New York, pp. 458–478.

Almar, R., Bonneton, P., Michallet, H., Cienfuegos, R., Ruessink, B.G., Tissier, M.F.S., 2013. On the use of the radon transform in studying nearshore wave dynamics: application to GLOBEX laboratory data. In: Proc. Coastal Dynamics.

Almar, R., Michallet, H., Cienfuegos, R., Bonneton, P., Tissier, M.F.S., Ruessink, B.G., 2014. On the use of the radon transform in studying nearshore wave dynamics. Coast. Eng. 92, 24–30.

Almeida, L., Masselink, G., Russell, P., Davidson, M., 2015. Observations of gravel beach dynamics during high energy wave conditions using a laser scanner. Geomorphology 228, 15–27. https://doi.org/10.1016/j.geomorph.2014.08.019.

Alsina, J.M., Cáceres, I., 2011. Sediment suspension events in the inner surf and swash zone. Measurements in large-scale and high-energy wave conditions. Coast. Eng. 58, 657–670. https://doi.org/10.1016/j.coastaleng.2011.03.002.

Anschutz, P., Smith, T., Mouret, A., Deborde, J., Bujan, S., Poirier, D., Lecroart, P., 2009. Tidal sands as biogeochemical reactors. Estuar. Coast. Shelf Sci. 84, 84–90.

Ardhuin, F., Devaux, E., Pineau-Guillou, L., 2010. Observation et prévision des seiches sur la côte atlantique française. XIèmes Journées Nationales" Génie Civil-Génie Côtier 22–24.

Ardhuin, F., Gualtieri, L., Stutzman, E., 2015. How ocean waves rock the earth: two mechanisms explain microseisms with periods 3 to 300 s. Geophys. Res. Lett. 42, https://doi.org/10.1002/2014GL062782.

Ardhuin, F., Herbers, T.H.C., 2013. Noise generation in the solid earth, oceans and atmosphere, from nonlinear interacting surface gravity waves in finite depth. J. Fluid Mech. 716, 316–348. https://doi.org/10.1017/jfm.2012.548.

Ardhuin, F., Rawat, A., Aucan, J., 2014. A numerical model for free infragravity waves: definition and validation at regional and global scales. Ocean Model. 77, 20–32.

Ardhuin, F., Roland, A., 2013. The development of spectral wave models: coastal and coupled aspects. In: Proceedings of Coastal Dynamics, p. 7th.

Arozarena, I., Houser, C., Echeverria, A., Brannstrom, C., 2015. The rip current hazard in Costa Rica. Nat. Hazards 77, 753–768. https://doi.org/10.1007/s11069-015-1626-9.

Artru, J., Ducic, V., Kanamori, H., Lognonn'e, P., Murakami, M., 2005. Ionospheric detection of gravity waves induced by tsunamis. Geophys. J. Int. 160, 840–848. https://doi.org/10.1111/j.1365-246X.2005.02552.x.

Aucan, J., Ardhuin, F., 2013. Infragravity waves in the deep ocean: an upward revision. Geophys. Res. Lett. 40, 3435–3439. https://doi.org/10.1002/grl.50321.

Austin, M., Scott, T.M., Brown, J.W., Brown, J.A., MacMahan, J.H., Masselink, G., Russell, P., 2010. Temporal observations of rip current circulation on a macro-tidal beach. Cont. Shelf Res. 30, 1149–1165.

Bakhtyar, R., Brovelli, A., Barry, D.A., Li, L., 2011. Wave-induced water table fluctuations, sediment transport and beach profile change: modeling and comparison with large-scale laboratory experiments. Coast. Eng. 58, 103–118.

Baldock, T., Simmonds, D., 1999. Separation of incident and reflected waves over sloping bathymetry. Coast. Eng. 38, 167–176. https://doi.org/10.1016/S0378-3839(99)00046-0, (cited By 32).

Baldock, T.E., 2012. Dissipation of incident forced long waves in the surf zone - implications for the concept of bound wave release at short wave breaking. Coast. Eng. 60, 276–285.

Baldock, T.E., Holmes, P., Horn, D., 1997. Low frequency swash motion induced by wave grouping. Coast. Eng. 32, 197–222.

Baldock, T.E., Huntley, D.A., 2002. Long wave forcing by the breaking of random waves on a beach. Proc. R. Soc. Lond. A. 258, 2177–2202.

Baldock, T.E., Huntley, D.A., Bird, P.A.D., O'Hare, T., Bullock, G.N., 2000. Breakpoint generated surf beat induced by bichromatic wave groups. Coast. Eng. 39, 213–242.

Baldock, T.E., Manoonvoravong, P., Pham, K.S., 2010. Sediment transport and beach morphodynamics induced by free long waves, bound long waves and wave groups. Coast. Eng. 57, 898–916. https://doi.org/10.1016/j.coastaleng.2010.05.006.

Battjes, J.A., Bakkenes, H.J., Janssen, T.T., van Dongeren, A.R., 2004. Shoaling of subharmonic gravity waves. J. Geophys. Res. 109, https://doi.org/10.1029/2003JC001863, C02009.

Baumann, J., Chaumillon, E., Bertin, X., Schneider, J.-L., Guillot, B., Schmutz, M., 2017. Importance of infragravity waves for the generation of washover deposits. Mar. Geol. 391, 20–35.

Beach, R.A., Sternberg, R.W., 1988. Suspended sediment transport in the surf zone: response to cross-shore infragravity motion. Mar. Geol. 80, 61–79.

Beetham, E., Kench, P., 2011. Field observations of infragravity waves and their behaviour on rock shore platforms. Earth Surf. Process. Landf. 36, 1872–1888. https://doi.org/10.1002/esp.2208.

Beetham, E., Kench, P., O'Callaghan, J., Popinet, S., 2016. Wave transformation and shoreline water level on Funafuti Atoll, Tuvalu. J. Geophys. Res. Oceans 121, 311–326. https://doi.org/10.1002/2015JC011246.

Berkhoff, J., 1972. Computation of combined refraction-diffraction, paper presented at 13th international conference on coastal engineering. Coastal Eng. Res. Counc. Vancouver, BC, Canada

Bertin, X., Fortunato, A., Oliveira, A., 2009. A modeling-based analysis of processes driving wave-dominated inlets. Cont. Shelf Res. 29, 819–834. https://doi.org/10.1016/j.csr.2008.12.019.

Bertin, X., Olabarrieta, M., 2016. Relevance of infragravity waves at a wave-dominated inlet. J. Geophys. Res. (212), 5418–5435. https://doi.org/10.1002/2015JC011444.

Biesel, F., 1952. équations génŕales au second ordre de la houle irŕgulière. La Houille Blanche 7, 372–376.

Blenkinsopp, C., Matias, A., Howe, D., Castelle, B., Marieu, V., Turner, I., 2016. Wave runup and overwash on a prototype-scale sand barrier. Coast. Eng. 113, 88–103. https://doi.org/10.1016/j.coastaleng.2015.08.006, Barrier Dynamics Experiment II: sediment processes across a large-scale sand barrier.

Boers, M., 1996. Simulation of a surf zone with a barred beach. 1. Wave heights and wave breaking. Communications on Hydraulic and Geotechnical Engineering, Report No. 96-5. Delft University of Technology, Netherlands.

Bonjean, D., Foray, P., Piedra-Cueva, I., Mory, M., Michallet, H., Breul, P., Haddani, Y., Abadie, S., et al., 2004. Monitoring of the foundations of a coastal structure submitted to breaking waves: occurrence of momentary liquefaction. In: The Fourteenth International Offshore and Polar Engineering Conference.

Bonneton, P., 2007. Modelling of periodic wave transformation in the inner surf zone. Ocean Eng. 34, 1459–1471.

Bonneton, P., Barthelemy, E., Chazel, F., Cienfuegos, R., Lannes, D., Marche, F., Tissier, M., 2011. Recent advances in Serre-Green Naghdi modelling for wave transformation, breaking and runup processes. Eur. J. Mech. B. Fluids 30, 589–597. https://doi.org/10.1016/j.euromechflu.2011.02.005.

Bonneton, P., Dupuis, H., 2001. Transformation of irregular waves in the inner surf zone. In: Coastal Engineering 2000. pp. 745–754. https://doi.org/10.1061/40549(276)58.

Bowen, A., Huntley, D., 1984. Waves, long waves and nearshore morphology. In: Greenwood, B., Davis Jr., R. (Eds.), Hydrodynamics and Sedimentation in Wave-Dominated Coastal Environments. Mar. Geol., vol. 60, pp. 1–13.

Bowen, A.J., 1969. Rip currents: 1. Theoretical investigations. J. Geophys. Res. 74, 5479–5490.
Bowen, A.J., Guza, R., 1978. Edge waves and surf beat. J. Geophys. Res. 83, 1913–1920.
Bowen, A.J., Inman, D.L., 1971. Edge waves and crescentic bars. J. Geophys. Res. 76, 8662–8671.
Bradshaw, M.P., 1980. Topographic control of run-up variability. In: Coastal Engineering 1980. pp. 1091–1105. https://doi.org/10.1061/9780872622647.067.
Brewster, B.C., 2010. Rip current misunderstanding. Nat. Hazards 55, 161–162.
Bricker, J.D., Roeber, V., 2015. Mechanisms of damage during Typhoon Haiyan: storm surge, waves, and 'tsunami-like' surf beat. In: E-proceedings of the 36th IAHR World Congress.
Brocchini, M., Baldock, T.E., 2008. Recent advances in modeling swash zone dynamicsmahan influence of surf-swash interaction on nearshore hydrodynamics and morphodynamics. Rev. Geophys. 46, https://doi.org/10.1029/2006RG000215, (n/a–n/a).
Bromirski, P.D., 2009. Earth vibrations. Science 324, 1026–1027. https://doi.org/10.1126/science.1171839.
Bromirski, P.D., Diez, A., Gerstoft, P., Stephen, R.A., Bolmer, T., Wiens, D.A., Aster, R.C., Nyblade, A., 2015. Ross ice shelf vibrations. Geophys. Res. Lett. 42, 7589–7597. https://doi.org/10.1002/2015GL065284.
Bruneau, N., Bertin, X., Castelle, B., Bonneton, P., 2014. Tide-induced flow signature in rip currents on a meso-macrotidal beach. Ocean Model. 74, 53–59.
Bruneau, N., Fortunato, A., Dodet, G., Freire, P., Oliveira, A., Bertin, X., 2011. Future evolution of a tidal inlet due to changes in wave climate, sea level and lagoon morphology (Óbidos lagoon, Portugal). Cont. Shelf Res. 31, 1915–1930.
Bryan, K.R., Howd, P.A., Bowen, A.J., 1998. Field observations of bar-trapped edge waves. J. Geophys. Res. 103, 1285–1305.
Burnett, W., Aggarwal, P., Aureli, A., Bokuniewicz, H., Cable, J., Charette, M., Kontar, E., Krupa, S., Kulkarni, K., Loveless, A., et al., 2006. Quantifying submarine groundwater discharge in the coastal zone via multiple methods. Sci. Total Environ. 367, 498–543.
Butt, T., Russell, P., Turner, I., 2001. The influence of swash infiltration-exfiltration on beach face sediment transport: onshore or offshore?. Coast. Eng. 42, 35–52.
Cañizares, R., Irish, J., 2008. Simulation of storm-induced barrier island morphodynamics and flooding. Coast. Eng. 55, 1089–1101. https://doi.org/10.1016/j.coastaleng.2008.04.006.
Cartwright, N., Baldock, T.E., Nielsen, P., Jeng, D.-S., Tao, L., 2006. Swash-aquifer interaction in the vicinity of the water table exit point on a sandy beach. J. Geophys. Res. Oceans 111.
Castelle, B., Coco, G., 2013. Surf zone flushing on embayed beaches. Geophys. Res. Lett. 40, 1–5. https://doi.org/10.1002/grl.50485.
Castelle, B., Marieu, V., Bujan, S., Splinter, K.D., Robinet, A., Senechal, N., Ferreira, S., 2015. Impact of the winter 2013–2014 series of severe Western Europe storms on a double-barred sandy coast: beach and dune erosion and megacusp embayments. Geomorphology 238, 135–148.
Castelle, B., McCarroll, R.J., Brander, R.W., Scott, T., Dubarbier, B., 2016. Modelling the alongshore variability of optimum rip current escape strategies on a multiple rip-channelled beach. Nat. Hazards 81, 663–686. https://doi.org/10.1007/s11069-015-2101-3.
Castelle, B., Scott, T., Brander, R.W., McCarroll, R.J., 2016. Rip current types, circulation and hazard. Earth-Sci. Rev. 163, 1–21.
Cheriton, O.M., Storlazzi, C.D., Rosenberger, K.J., 2016. Observations of wave transformation over a fringing coral reef and the importance of low-frequency waves and offshore water levels to runup, overwash, and coastal flooding. J. Geophys. Res. Oceans 121 (5), 3121–3140. https://doi.org/10.1002/2015JC011231.
Coco, G., Murray, A.B., 2008. Patterns in the sand: from forcing templates to self-organization. Geomorphology 91, 271–290.
Collis, W.B., White, P.R., Hammond, J.K., 1998. Higher-order spectra: the bispectrum and trispectrum. Mech. Syst. Signal Process. 12 (3), 375–394.
Conley, D.C., Beach, R.A., 2003. Cross-shore sediment transport partitioning in the nearshore during a storm event. J. Geophys. Res. 108, C06011, 10.1029/2001JC001230.
Contardo, S., Symonds, G., 2013. Infragravity response to variable wave forcing in the nearshore. J. Geophys. Res. 118, 7095–7106. https://doi.org/10.1002/2013JC009430.
Crawford, W., Ballu, V., Bertin, X., Karpytchev, M., 2015. The sources of deep ocean infragravity waves observed in the North Atlantic ocean. J. Geophys. Res. 120, 5120–5133. https://doi.org/10.1002/2014JC010657.
Crawford, W.C., Webb, S.C., Hildebrand, J.A., 1991. Seafloor compliance observed by long-period pressure and displacement measurements. JGR 103, 9895–9916.
Dalrymple, R.A., MacMahan, J.H., Reniers, A.J.H.M., Nelko, V., 2011. Rip currents. Annu. Rev. Fluid Mech. 43, 551–581. https://doi.org/10.1146/annurev-fluid-122109-160733.
Darcy, H., 1856. Les fontaines publiques de la ville de Dijon: exposition et application. Victor Dalmont.
Davis, W., 1925. The undertow myth. Science 61, 206–208.
Davy, C., Barruol, G., Fontaine, F.R., Sigloch, K., Stutzmann, E., 2014. Tracking major storms from microseismic and hydroacoustic observations on the seafloor. Geophys. Res. Lett. 41, 8825–8831. https://doi.org/10.1002/2014GL062319.
De Bakker, A.T.M., Brinkkemper, J.A., van der Steen, F., Tissier, M.F.S., Ruessink, B.G., 2016. Cross-shore sand transport by infragravity waves as a function of beach steepness. J. Geophys. Res. Earth Surf.(in press).
De Bakker, A.T.M., Herbers, T.H.C., Smit, P.B., Tissier, M.F.S., Ruessink, B.G., 2015. Nonlinear infragravity-wave interactions on a gently sloping laboratory beach. J. Phys. Oceanogr. 45, 589–605. https://doi.org/10.1175/JPO-D-14-0186.1.
De Bakker, A.T.M., Tissier, M.F.S., Marieu, V., Sénéchal, N., Ruju, A., Lara, J., Ruessink, B.G., 2013. Infragravity wave propagation and dissipation on a low-sloping laboratory beach. In: Proc. 7th Int. Conf. on Coastal Dynamics. pp. 443–452.
De Bakker, A.T.M., Tissier, M.F.S., Ruessink, B.G., 2014. Shoreline dissipation of infragravity waves. Cont. Shelf Res. 72, 73–82. https://doi.org/10.1016/j.csr.2013.11.013.
De Bakker, A.T.M., Tissier, M.F.S., Ruessink, B.G., 2015. Beach steepness effects on nonlinear infragravity-wave interactions: a numerical study. J. Geophys. Res. 121, https://doi.org/10.1002/2015JC011268.
De Jong, M., Battjes, J., 2004. Low-frequency sea waves generated by atmospheric convection cells. J. Geophys. Res. Oceans 109.
Dodet, G., Bertin, X., Bruneau, N., Fortunato, A., Nahon, A., Roland, A., 2013. Wave-current interactions in a wave-dominated tidal inlet. J. Geophys. Res. Oceans 118, 1587–1605. https://doi.org/10.1002/jgrc.20146.
Earlie, C., Young, A., Masselink, G., Russell, P., 2015. Coastal cliff ground motions and response to extreme storm waves. Geophys. Res. Lett. 42, 847–854. https://doi.org/10.1002/2014GL062534.
Eckart, C., 1951. Surface waves on water of variable depth. In: Technical Report. University of California, Scripps.
Elgar, S., Guza, R.T., 1985. Observations of bispectra of shoaling surface gravity waves. J. Fluid Mech. 161, 425–448.
Elgar, S., Guza, R.T., 1988. Statistics of bicoherence. IEEE Trans. Acoust. Speech Signal Process. 36, 1667–1668.
Elgar, S., Herbers, T.H.C., Guza, R.T., 1994. Reflection of ocean surface gravity waves from a natural beach. J. Phys. Oceanogr. 24, 1503–1511. https://doi.org/10.1175/1520-0485(1994)024<1503:ROOSGW>2.0.CO;2.
Elgar, S., Herbers, T.H.C., Okihiro, M., Oltman-Shay, J., Guza, R.T., 1992. Observations of infragravity waves. J. Geophys. Res. 97 (C10), 15573–15577.
Falqueś, A., Coco, G., Huntley, D., 2000. A mechanism for the generation of wave-driven rhythmic patterns in the surf zone. J. Geophys. Res. 105, 24071–24088.
Feddersen, F., 2014. The generation of surfzone eddies in a strong alongshore current. J. Phys. Oceanogr. 44, 600–617.
Ferrario, F., Beck, M., Storlazzi, C., Micheli, F., Shepard, C., Airoldi, L., 2014. The effectiveness of coral reefs for coastal hazard risk reduction and adaptation. Nat. Commun. 5, https://doi.org/10.1038/ncomms4794.
Fiedler, J.W., Brodie, K.L., McNinch, J.E., Guza, R.T., 2015. Observations of runup and energy flux on a low-slope beach with high-energy, long-period ocean swell. Geophys. Res. Lett. 42, https://doi.org/10.1002/2015GL066124.
Freilich, M.H., Guza, R.T., 1984. Nonlinear effects on shoaling surface gravity waves. Phil. Trans. R. Soc. Lond. A311, 1–41.
Frigaard, P., Brorsen, M., 1995. A time-domain method for separating incident and reflected irregular waves. Coast. Eng. 24, 205–215. https://doi.org/10.1016/0378-3839(94)00035-V.
Gaillard, P., Gauthier, M., Holly, F., 1980. Method of analysis of random wave experiments with reflecting coastal structures. In: Proceedings of the 17th Conference on Coastal Engineering, ASCE, New York.
Gallagher, B., 1971. Generation of surf beat by non-linear wave interactions. J. Fluid Mech. 49, 1–20.
Gawehn, M., van Dongeren, A., van Rooijen, A., Storlazzi, C., Cheriton, O., Reniers, A., 2016. Identification and classification of very low frequency waves on a coral reef flat. J. Geophys. Res. Oceans 121, 7560–7574. https://doi.org/10.1002/2016JC011834.
Geng, X., Boufadel, M.C., 2015. Numerical study of solute transport in shallow beach aquifers subjected to waves and tides. J. Geophys. Res. Oceans 120, 1409–1428.
Gensini, V.A., Ashley, W.S., 2009. An examination of rip current fatalities in the United States. Nat. Hazards 54, 159–175.
Giese, G.S., Chapman, D.C., 1993. Coastal seiches. Oceanus 36, 38–46.
Goda, Y., Suzuki, Y., 1976. Estimation of incident and reflected waves in random wave experiments. In: Proceedings of the 15th Conference on Coastal Engineering, ASCE, New York..
Godin, O.A., Zabotin, N.A., Bullett, T.W., 2015. Acoustic-gravity waves in the atmosphere generated by infragravity waves in the ocean. Earth Planets Space 47, https://doi.org/10.1186/s40623–015-0212-4.
Godin, O.A., Zabotin, N.A., Sheehan, A.F., Collins, J.A., 2014. Interferometry of infragravity waves off New Zealand. J. Geophys. Res. 119, 1103–1122. https://doi.org/10.1002/2013JC009395.
Guedes, M.C., Bryan, K.R., Coco, G., 2013. Observations of wave energy fluxes and swash motions on a low-sloping, dissipative beach. J. Geophys. Res. 118, 3651–3669. https://doi.org/10.1002/jgrc.20267.
Guyon, E., Hulin, J.-P., Petit, L., Mitescu, C.D., 2015. Physical hydrodynamics. OUP Oxford.
Guza, R.T., Davis, R.E., 1974. Excitation of edge waves by waves incident on a beach. J. Geophys. Res. 79, 1285–1291.
Guza, R.T., Feddersen, F., 2012. Effect of wave frequency and directional spread on shoreline runup. Geophys. Res. Lett. 39, L11607. https://doi.org/10.1029/2012GL051959.
Guza, R.T., Thornton, E.B., 1982. Swash oscillations on a natural beach. J. Geophys. Res. 87, 483–491.
Guza, R.T., Thornton, E.B., 1985. Observations of surf beat. J. Geophys. Res. 87, 483–491.

Guza, R.T., Thornton, E.B., Holman, R.A., 1984. Swash on steep and shallow beaches. In: Proceedings of the 19th International Conference on Coastal Engineering, ASCE. pp. 708–723.
Hardy, T., Young, I., 1996. Field study of wave attenuation on an offshore coral reef. J. Geophys. Res. C: Oceans 101, 14311–14326, (Cited By 82).
Hasselmann, K., 1962. On the non-linear energy transfer in a gravity-wave spectrum Part 1. General theory. J. Fluid Mech. 12, 481–500.
Hasselmann, K., 1963. A statistical analysis of the generation of microseisms. Rev. Geophys. 1, 177–210.
Hasselmann, K., 1966. Feynman diagrams and interaction rules of wave-wave scattering processes. Rev. Geophys. 4, 1–32.
Hasselmann, K., Munk, W., MacDonald, G., 1963. Bispectra of ocean waves. In: Rosenblatt, M. (Ed.), Time Series Analysis. John Wiley, New York.
Haubrich, R., 1965. Earth noises, 5 to 500 millicycles per second, 1. J. Geophys. Res. 70, 1415–1427.
Heiss, J.W., Puleo, J.A., Ullman, W.J., Michael, H.A., 2015. Coupled surface-subsurface hydrologic measurements reveal infiltration, recharge, and discharge dynamics across the swash zone of a sandy beach. Water Resour. Res. https://doi.org/10.1002/2015WR017395.
Henderson, S., Elgar, S., Bowen, A., 2000. Observations of surf beat propagation and energetics. In: pp. 1412–1421.
Henderson, S.M., Bowen, A.J., 2002. Observations of surf beat forcing and dissipation. J. Geophys. Res. 107 (C11), 3193. https://doi.org/10.1029/2000JC000498.
Henderson, S.M., Guza, R.T., Elgar, S., Herbers, T.H.C., Bowen, A.J., 2006. Nonlinear generation and loss of infragravity wave energy. J. Geophys. Res. 111, C12007. https://doi.org/10.1029/2006JC003539.
Herbers, T.H.C., Burton, M.C., 1997. Nonlinear shoaling of directionally spread waves on a beach. J. Geophys. Res. 102, 21101–21114.
Herbers, T.H.C., Elgar, S., Guza, R.T., 1994. Infragravity-frequency (0.005–0.05 Hz) Motions on the shelf. Part I : Forced Waves. J. Phys. Oceanogr. 24, 917–927.
Herbers, T.H.C., Elgar, S., Guza, R.T., 1995. Generation and propagation of infragravity waves. J. Geophys. Res. 100, 24863–24872.
Herbers, T.H.C., Orzech, M., Elgar, S., Guza, R.T., 2003. Shoaling transformation of wave-frequency directional spectra. J. Geophys. Res. 108, https://doi.org/10.1029/2001JC001304.
Herbers, T.H.C., Russnogle, N.R., Elgar, S., 2000. Spectral energy balance of breaking waves within the surf zone. J. Phys. Oceanogr. 30, 2723–2737.
Hibberd, S., Peregrine, D., 1979. Surf and run-up on a beach: a uniform bore. J. Fluid Mech. 95, 323–345.
Hoeke, R., McInnes, K., Kruger, J., McNaught, R., Hunter, J., Smithers, S., 2013. Widespread inundation of pacific islands triggered by distant-source wind-waves. Glob. Planet. Chang. 108, 1–11. https://doi.org/10.1016/j.gloplacha.2013.06.006.
Holland, K.T., Holman, R.A., 1999. Wavenumber-frequency structure of infragravity swash motions. J. Geophys. Res. 104, 13479–13488.
Holman, R.A., 1981. Infragravity energy in the surf zone. J. Geophys. Res. 86, 6442–6450.
Holman, R.A., Bowen, A., 1982. Bars, bumps and holes: models for the generation of complex beach topography. J. Geophys. Res. 87, 457–468.
Holman, R.A., Bowen, A.J., 1979. Edge waves on complex beach profiles. J. Geophys. Res. 84, 6339–6346.
Holman, R.A., Sallenger, A.H., 1985. Setup and swash on a natural beach. J. Geophys. Res. 90, 945–953.
Horn, D.P., 2006. Measurements and modelling of beach groundwater flow in the swash-zone: a review. Cont. Shelf Res. 26, 622–652.
Houser, C., Greenwood, B., 2005. Hydrodynamics and sediment transport within the inner surf zone of a lacustrine multiple-barred nearshore. Mar. Geol. 218, 37–63. https://doi.org/10.1016/j.margeo.2005.02.029.
Howd, P.A., Oltman-Shay, J., Holman, R.A., 1991. Wave variance partitioning in the trough of a barred beach. J. Geophys. Res. 96, 12781–12795.
Howd, P.A., Bowen, A.J., Holman, R.A., 1992. Edge waves in the presence of strong longshore currents. J. Geophys. Res. 97, 11357–11371.
Huntley, D., Bowen, A., 1974. Field measurements of nearshore velocities. In: Coastal Engineering 1974. pp. 538–557. https://doi.org/10.1061/9780872621138.033.
Huntley, D., Bowen, A., 1975. Comparison of the Hydrodynamics of Steep and Shallow Beaches. John Wiley & Sons.
Huntley, D., Davidson, M., Russell, P., Foote, Y., Hardisty, J., 1993. Long waves and sediment movement on beaches: recent observations and implications for modelling. J. Coast. Res. SI 15, 215–229.
Huntley, D.A., Guza, R.T., Thornton, E.B., 1981. Field observations of surf beat: 1. Progressive edge waves. J. Geophys. Res. Oceans 86, 6451–6466. https://doi.org/10.1029/JC086iC07p06451.
Huntley, D.A., Hanes, D.M., 1987. Direct measurements of suspended sediment transport. In: ASCE (Ed.), Coastal Sediments. pp. 723–737.
Huntley, D.A., Simmonds, D., Tatavarti, V.S.N., 1999. Use of collocated sensors to measure coastal wave reflection. J. Waterw. Port Coast. Ocean Eng. 125, 46–52.
Inch, K., Davidson, M., Masselink, G., Russell, P., 2017. Correcting wave reflection estimates in the coastal zone. Coast. Eng.65–71.
Inch, K., Davidson, M., Masselink, G., Russell, P., 2017. Observations of nearshore infragravity wave dynamics under high energy swell and wind-wave conditions. Cont. Shelf Res. 138, 19–31. https://doi.org/10.1016/j.csr.2017.02.010.
Iribarren, C., Nogales, C., 1949. Protection des Ports. In: XVIIth International Navigation Congress. pp. 31–80, (Lisbon, Portugal).
Jaffe, B., Richmond, B., 1992. Overwash variability on the shoreline of Guam during Typhoon Russ. In: Proceedings of 7th International Coral Reef Symposium. 1, pp. 257–264.
Janssen, T.T., 2006. Nonlinear Surface Waves over Topography. Technical University of Delft, The Netherlands, (Ph.D. thesis).
Janssen, T.T., Battjes, J.A., van Dongeren, A.R., 2003. Long waves induced by short-wave groups over a sloping bottom. J. Geophys. Res. 108, 3252. https://doi.org/10.1029/2002JC001515.
Karambas, T.V., 2003. Modelling of infiltration-exfiltration effects of cross-shore sediment transport in the swash zone. Coast. Eng. J. 45, 63–82.
Kennedy, A.B., Chen, Q., Kirby, J.T., Dalrymple, R.A., 2000. Boussinesq modeling of wave transformation, breaking, and runup. I: 1D. J. Waterw. Port Coast. Ocean Eng. 126, 39–47.
Kim, Y., Powers, E., 1979. Digital bispectral analysis and its application to nonlinear wave interactions. IEEE Trans. Plasma Sci. 1, 120–131.
Kostense, J.K., 1984. Measurement of surf beat and set-down beneath wave groups. In: ASCE (Ed.), Proceedings of the 19th International Conference on Coastal Engineering. pp. 724–740.
Kularatne, S., Pattiaratchi, C., 2014. The role of infragravity waves in near-bed cross-shore sediment flux in the breaker zone. J. Mar. Sci. Eng. 2, 568–592. https://doi.org/10.3390/jmse20300568.
Lara, J.L., Ruju, A., Losada, I.J., 2010. Reynolds averaged Navier-Stokes modelling of long waves induced by a transient wave group on a beach. Proc. R. Soc. Lond. A: Math. Phys. Eng. Sci. https://doi.org/10.1098/rspa.2010.0331, (rspa20100331).
Larsen, L., 1982. A new mechanism for seaward dispersion of midshelf sediments. Sedimentology 29, 279–283.
Lee, J.-J., 1971. Wave-induced oscillations in harbours of arbitrary geometry. J. Fluid Mech. 45, 375–394.
Lee, K.-H., Mizutani, N., Hur, D.-S., Kamiya, A., 2007. The effect of groundwater on topographic changes in a gravel beach. Ocean Eng. 34, 605–615.
Li, L., Barry, D., 2000. Wave-induced beach groundwater flow. Adv. Water Resour. 23, 325–337.
Lin, Y.-H., Hwung, H.-H., 2012. Infra-gravity wave generation by the shoaling wave groups over beaches. China Ocean Eng. 26, 1–18.
Lippmann, T.C., Holman, R.A., 1990. The spatial and temporal variability of sand bar morphology. J. Geophys. Res. 95, 11575–11590.
List, J., 1992. A model for the generation of two-dimensional surf beat. J. Geophys. Res. 97, 5623–5635, (Cited By 0).
List, J.H., 1991. Wave groupiness variations in the nearshore. Coast. Eng. 15 (5–6), 475–496.
Long, J.W., Ozkan-Haller, H.T., 2005. Offshore controls on nearshore rip currents. J. Geophys. Res. 110 (C12007)https://doi.org/10.1029/2005JC003018.
Longuet-Higgins, M., Stewart, R., 1962. Radiation stress and mass transport in gravity waves, with application to surf beats. J. Fluid Mech. 13, 481–504. https://doi.org/10.1017/S0022112062000877.
Loureiro, C., Ferreira, O., Cooper, J.A.G., 2012. Extreme erosion on high-energy embayed beaches: influence of megarips and storm grouping. Geomorphology 139–140, 155–171.
Lowe, R., Falter, J., Bandet, M., Pawlak, G., Atkinson, M., Monismith, S., Koseff, J., 2005. Spectral wave dissipation over a barrier reef. J. Geophys. Res. C: Oceans 110, 1–16. https://doi.org/10.1029/2004JC002711.
MacMahan, J., Thornton, E., Reniers, A., 2006. Rip current review. Coast. Eng. 53, 191–208. https://doi.org/10.1016/j.coastaleng.2005.10.009.
MacMahan, J.H., Reniers, A.J.H.M., Thornton, E.B., Stanton, T.P., 2004. Infragravity rip current pulsations. J. Geophys. Res. 109, https://doi.org/10.1029/2003JC002068.
Mansard, E., Funke, E., 1980. The measurement of incident and reflected spectra using a least squares method. In: Proceedings of the 17th Conference on Coastal Engineering, ASCE, New York.
Marche, F., Bonneton, P., Fabrie, P., Seguin, N., 2007. Evaluation of well-balanced bore-capturing schemes for 2D wetting and drying processes. Int. J. Numer. Methods Fluids 53, 867–894.
Marshall, R., Stephenson, W., 2011. The morphodynamics of shore platforms in a micro-tidal setting: interactions between waves and morphology. Mar. Geol. 288, 18–31. https://doi.org/10.1016/j.margeo.2011.06.007, (cited By 23).
Martins, K., Blenkinsopp, C., Power, H., Bruder, B., Puleo, J., Bergsma, E., 2017. High-resolution monitoring of wave transformation in the surf zone using a LiDAR scanner array. 128, 37–43.
Mase, H., 1989. Random wave runup height on gentle slope. J. Waterw. Port Coast. Ocean Eng. 115, 649–661.
Mase, H., 1995. Frequency down-shift of swash oscillations compared to incident waves. J. Hydraul. Res. 33, 397–411. https://doi.org/10.1080/00221689509498580.
Mase, H., Iwagaki, Y., 1984. Run-up of random waves on gentle slopes. Coast. Eng. Proc. 1, 593–609.
Masselink, G., 1995. Group bound long waves as a source of infragravity energy in the surf zone. Cont. Shelf Res. 15, 1525–1547. https://doi.org/10.1016/0278-4343(95)00037-2, (cited By 0).
Matias, A., Williams, J., Masselink, G., Ferreira, O., 2012. Overwash threshold for gravel barriers. Coast. Eng. 63, 48–61.
McAllister, S.M., Barnett, J.M., Heiss, J.W., Findlay, A.J., MacDonald, D.J., Dow, C.L., Luther, G.W., Michael, H.A., Chan, C.S., 2015. Dynamic hydrologic and biogeochemical processes drive microbially enhanced iron and sulfur cycling within the intertidal mixing zone of a beach aquifer. Limnol. Oceanogr. 60, 329–345.
McCall, R., 2015. Process-based Modelling of Storm Impacts on Gravel Coasts. Plymouth University, UK, (Ph.D. thesis).

McCall, R., Van Thiel de Vries, J.S.M., Plant, N., Van Dongeren, A.R., Roelvink, J.A., Thompson, D., Reniers, A., 2010. Two-dimensional time dependent hurricane overwash and erosion modeling at Santa Rosa Island. Coast. Eng. 57, 668–683. https://doi.org/10.1016/j.coastaleng.2010.02.006.

McCarroll, R.J., Brander, R.W., Turner, I.L., Power, H.E., Mortlock, T.R., 2014. Lagrangian observations of circulation on an embayed beach with headland rip currents. Mar. Geol. 355, 173–188. https://doi.org/10.1016/j.margeo.2014.05.020.

Merrifield, M.A., Becker, J., Ford, M., Yao, Y., 2014. Observations and estimates of wave-driven water level extremes at the Marshall Islands. Geophys. Res. Lett. 41 (20), 7245–7253. https://doi.org/10.1002/2014GL061005.

Michallet, H., Mory, M., Piedra-Cueva, I., 2009. Wave-induced pore pressure measurements near a coastal structure. J. Geophys. Res. Oceans 114.

Monismith, S.G., Rogers, J.S., Koweek, D., Dunbar, R.B., 2015. Frictional wave dissipation on a remarkably rough reef. Geophys. Res. Lett. 42, 4063–4071. https://doi.org/10.1002/2015GL063804, 2015GL063804.

Muller, H., Van Rooijen, A., Idier, D., Pedreros, R., 2016. Storm impact on a French coastal dune system: morphodynamic modeling using X-beach. In: Infra-gravity waves : from driving mechanisms to impacts. https://hal-brgm.archives-ouvertes.fr/hal-01275253, La Rochelle, France.

Munk, W., 1949. Surf beat. Eos Trans. AGU 30, 849–854.

Munk, W., Sargent, M., 1948. Adjustment of Bikini Atoll to ocean waves. Eos Trans. AGU 29, 855–860. https://doi.org/10.1029/TR029i006p00855.

Nahon, A., Bertin, X., Fortunato, A., Oliveira, A., 2012. Process-based 2DH morphodynamic modeling of tidal inlets: a comparison with empirical classifications and theories. Mar. Geol. 291–294, 1–11. https://doi.org/10.1016/j.margeo.2011.10.001.

Nawa, K., Suda, N., Fukao, Y., Sato, T., Aoyama, Y., Shibuya, K., 1998. Incessant excitation of the Earth's free oscillations. Earth Planets Space 50, 3–8. https://doi.org/10.1029/2006GC001274.

Nazaka, E., Hino, M., 1991. Bore-like surf beat in a reef zone caused by wave groups of incident short period waves. Fluid Dyn. Res. 7, 89–100.

Neale, J., Harmon, N., Srokosz, M., 2015. Source regions and reflection of infragravity waves offshore of the U.S. Pacific Northwest. J. Geophys. Res. 120, 1–18.

Nielsen, P., 1990. Tidal dynamics of the water table in beaches. Water Resour. Res. 26, 2127–2134.

Nishida, K., 2013. Earth's background free oscillations. Annu. Rev. Earth Planet. Sci. 41, 719–740.

van Noorloos, J.C., 2003. Energy Transfer Between Short Wave Groups and Bound Long Waves on a Plane Slope. Master's thesis. Delft University of technology, Delft, The Netherlands.

Norheim, C.A., Herbers, T.H.C., Elgar, S., 1998. Nonlinear evolution of surface wave spectra on a beach. J. Phys. Oceanogr. 28, 1534–1551.

Nwogu, O., Demirbilek, Z., 2010. Infragravity wave motions and runup over shallow fringing reefs. ASCE J. Waterw. Port Coast. Ocean Eng.

Ogawa, H., Dickson, M., Kench, P., 2011. Wave transformation on a sub-horizontal shore platform, Tatapouri, North Island, New Zealand. Cont. Shelf Res. 31, 1409–1419. https://doi.org/10.1016/j.csr.2011.05.006, Cited By 25.

Ogawa, H., Dickson, M., Kench, P., 2015. Hydrodynamic constraints and storm wave characteristics on a sub-horizontal shore platform. Earth Surf. Process. Landf. 40, 65–77. https://doi.org/10.1002/esp.3619.

Okihiro, M., Guza, R.T., 1995. Infragravity energy modulation by tides. J. Geophys. Res. Oceans 100, 16143–16148. https://doi.org/10.1029/95JC01545.

Okihiro, M., Guza, R.T., Seymour, R.J., 1993. Excitation of seiche observed in a small harbor. J. Geophys. Res. 98, 18.201–18.211.

Oltman-Shay, J., Guza, R.T., 1987. Infragravity edge wave observations on two california beaches. J. Phys. Oceanogr. 17, 644–663.

Oltman-Shay, J., Hathaway, K., 1989. Infragravity energy and its implications in nearshore sediment transport and sandbar dynamics, report number tr cerc-89-8. Department of the Army, waterways experiment stations, US Army Corps of Engineers.

Oltman-Shay, J., Howd, P.A., 1993. Edge waves on nonplanar bathymetry and alongshore currents: a model and data comparison. J. Geophys. Res. 98, 2495–2507.

Orescanin, M., Raubenheimer, B., Elgar, S., 2014. Observations of wave effects on inlet circulation. Cont. Shelf Res. 82, 37–42. https://doi.org/10.1016/j.csr.2014.04.010.

Osborne, P.D., Greenwood, B., 1992. Frequency dependent cross-shore suspended sediment transport. 2. A barred shoreface. Mar. Geol. 106, 25–51.

Özkan-Haller, H., Vidal, C., Losada, I.J., Medina, R., Losada, M.A., 2001. Standing edge waves on a pocket beach. J. Geophys. Res. Oceans 106, 16981–16996.

Ozkan-Haller, H.T., Kirby, J.T., 1999. Nonlinear shear instabilities of the longshore current: a comparison of observations and computations. J. Geophys. Res. 104, https://doi.org/10.1029/1999JC900104.

Péquignet, A., Becker, J., Merrifield, M., Aucan, J., 2009. Forcing of resonant modes on a fringing reef during tropical storm Man-yi. Geophys. Res. Lett. 36, https://doi.org/10.1029/2008GL036259.

Peregrine, D.H., 1974. Water-wave interaction in the surf zone. In: Coastal Engineering 1974. pp. 500–517. https://doi.org/10.1061/9780872621138.031.

Pomeroy, A., Lowe, R., Symonds, G., Van Dongeren, A., Moore, C., 2012. The dynamics of infragravity wave transformation over a fringing reef. J. Geophys. Res. 117, https://doi.org/10.1029/2012JC008310.

Pomeroy, A.W.M., Lowe, R.J., Van Dongeren, A.R., Ghisalberti, M., Bodde, W., Roelvink, D., 2015. Spectral wave-driven sediment transport across a fringing reef. Coast. Eng. 98, 78–94. https://doi.org/10.1016/j.coastaleng.2015.01.005.

Rabinovich, A., 2009. Seiches and harbor oscillations. https://doi.org/10.1142/9789812819307_0009.

Radon, J., 1917. Über die bestimmung von funktionen durch ihre integralwerte längs gewisser mannigfaltigkeiten. Berichte Sächsische Akademie der Wissenschaften, Leipzig, Math.-Phys.Kl. 69, 262–267.

Raubenheimer, B., Guza, R.T., 1996. Observations and predictions of run-up. J. Geophys. Res. 101, 25,575–25,587.

Raubenheimer, B., Guza, R.T., Elgar, S., 1996. Wave transformation across the inner surf zone. J. Geophys. Res. 101, 25589–25597.

Rawat, A., Ardhuin, F., Ballu, V., Crawford, W., Corela, C., Aucan, J., 2014. Infragravity waves across the oceans. Geophys. Res. Lett. 41, 7957–7963. https://doi.org/10.1002/2014GL061604, 2014GL061604.

Reniers, A., MacMahan, J., Thornton, E., Stanton, T., 2006. Modelling infragravity motions on a rip-channel beach. Coast. Eng. 53, 209–222. https://doi.org/10.1016/j.coastaleng.2005.10.010.

Reniers, A., MacMahan, J., Thornton, E., Stanton, T., Henriquez, M., Brown, J., Brown, J., Gallagher, E., 2009. Surf zone surface retention on a rip-channeled beach. J. Geophys. Res. Oceans 114, https://doi.org/10.1029/2008JC005153.

Reniers, A.J.H.M., van Dongeren, A.R., Battjes, J.A., Thornton, E.B., 2002. Linear modelling of infragravity waves during Delilah. J. Geophys. Res. 107, 3137. https://doi.org/10.1029/2001JC001083.

Reniers, A.J.H.M., Roelvink, J.A., Thornton, E.B., 2004. Morphodynamic modeling of an embayed beach under wave group forcing. J. Geophys. Res. 109, https://doi.org/10.1029/2002JC001586.

Rhie, J., Romanowicz, B., 2004. Excitation of earth's incessant free oscillations by atmosphere-ocean-seafloor coupling. Nature 431, 552–556.

Rhie, J., Romanowicz, B., 2006. A study of the relation between ocean storms and the Earth-s hum. Geochm. Geophys. Geosyst. 7, Q10004. https://doi.org/10.1029/2006GC001274.

Rijnsdorp, D.P., Ruessink, B.G., Zijlema, M., 2015. Infragravity-wave dynamics in a barred coastal region, a numerical study. J. Geophys. Res. 120 (6), 4068–4089. https://doi.org/10.1002/2014JC010450.

Roelvink, D., Reniers, A., van Dongeren, A., van Thiel de Vries, J., McCall, R., Lescinski, J., 2009. Modelling storm impacts on beaches, dunes and barrier islands. Coast. Eng. 56, 1133–1152.

Roelvink, J., 1993. Surf Beat and its Effect on Cross-shore Profiles. Ph.D. thesis.

Roelvink, J.A., Stive, M.J.F., 1989. Bar-generating cross-shore flow mechanisms on a beach. J. Geophys. Res. 94, 4785–4800.

Rogers, J., Monismith, S., Dunbar, R., Koweek, D., 2015. Field observations of wave-driven circulation over spur and groove formations on a coral reef. J. Geophys. Res. C: Oceans 120, 145–160. https://doi.org/10.1002/2014JC010464.

Ruessink, B.G., 1998. Bound and free infragravity waves in the nearshore zone under breaking and nonbreaking conditions. J. Geophys. Res. 103, 12.795–12.805.

Ruessink, B.G., 1998. The temporal and spatial variability of infragravity energy in a barred nearshore zone. Cont. Shelf Res. 18, 585–605.

Ruessink, B.G., Houwman, K.T., Hoekstra, P., 1998. The systematic contribution of transporting mechanisms to the cross-shore sediment transport in water depths of 3 to 9 m. Mar. Geol. 152, 295–324.

Ruessink, B.G., Kleinhans, M.G., Van den Beukel, P.G.L., 1998. Observations of swash under highly dissipative conditions. J. Geophys. Res. 103, 3111–3118.

Ruessink, B.G., Michallet, H., Bonneton, P., Mouazé, D., Lara, J.L., Silva, P.A., Wellens, P., 2013. Globex: wave dynamics on a gently sloping laboratory beach. In: Proc. Coastal Dynamics 2013. pp. 1351–1362.

Ruessink, B.G., Van Enckevort, I.M.J., Kingston, K.S., Davidson, M.A., 2000. Analysis of observed two- and three-dimensional nearshore bar behaviour. Mar. Geol. 169, 161–183a.

Ruggiero, P., Holman, R.A., Beach, R.A., 2004. Wave run-up on a high-energy dissipative beach. J. Geophys. Res. 109, C06025. https://doi.org/10.1029/2003JC002160.

Ruggiero, P., Komar, P., McDougal, W., Marra, J., Beach, R., 2001. Wave runup, extreme water levels and the erosion of properties backing beaches. J. Coast. Res. 17, 407–419.

Ruju, A., Lara, J.L., Losada, I.J., 2012. Radiation stress and low-frequency energy balance within the surf zone: a numerical approach. Coast. Eng. 68, 44–55.

Russell, P., 1993. Mechanisms for beach erosion during storm. Cont. Shelf Res. 13, 1243–1265.

Sakai, T., Hatanaka, K., Mase, H., 1992. Wave-induced effective stress in seabed and its momentary liquefaction. J. Waterw. Port Coast. Ocean Eng. 118, 202–206.

Sallenger, A., 2000. Storm impact scale for barrier islands. J. Coast. Res. 16, 890–895.

Sallenger, A.H., Holman, R.A., Birkemeier, W., 1985. Storm-induced response of a nearshore-bar system. Mar. Geol. 64, 237–257.

Sawyer, A.H., Lazareva, O., Kroeger, K.D., Crespo, K., Chan, C.S., Stieglitz, T., Michael, H.A., 2014. Stratigraphic controls on fluid and solute fluxes across the sediment-water interface of an estuary. Limnol. Oceanogr 59, 997–1010.

Schäffer, H.A., 1993. Infragravity waves induced by short wave groups. J. Fluid Mech. 247, 551–588.

Seelig, W.N., 1983. Laboratory study of reef-lagoon system hydraulics. J. Waterw. Port Coast. Ocean Eng. 109, 380–391. https://doi.org/10.1061/(ASCE)0733-950X(1983)109:4(380).

Sembiring, L., van Dongeren, A., Winter, G., Roelvink, D., 2016. Dynamic modelling of rip currents for swimmer safety on a wind-sea dominated mesotidal beach. J. Coast. Res. 32, 339–353. https://doi.org/10.2112/JCOASTRES-D-14-00260.1.

Sénéchal, N., Bonneton, P., Dupuis, H., 2001. Field observations of irregular wave transformation in the surf zone. Proc. Fourth Conf. Coast. Dyn.62–70.

Sénéchal, N., Coco, G., Bryan, K.R., Holman, R.A., 2011. Wave runup during extreme storm conditions. J. Geophys. Res. 116, C07032. https://doi.org/10.1029/2010JC006819.
Sénéchal, N., Dupuis, H., Bonneton, P., Howa, H., Pedreros, R., 2001. Observation of irregular wave transformation in the surf zone over a gently sloping sandy beach on the French Atlantic coastline. Oceanol. Acta 324, 545–556.
Shanks, A.L., Morgan, S.G., MacMahan, J.H., Reniers, A.J.H.M., 2010. Surf zone physical and morphological regime as determinants of temporal and spatial variation in larval recruitent. J. Exp. Mar. Biol. Ecol. 392, 140–150.
Sheremet, A., Davis, J., Tian, M., Hanson, J., Hathaway, K., 2016. Triads: a phase-resolving model for nonlinear shoaling of directional wave spectra. Ocean Model. 99, 60–74.
Sheremet, A., Guza, R.T., Elgar, S., Herbers, T.H.C., 2002. Observations of nearshore infragravity waves: seaward and shoreward propagating components. J. Geophys. Res. 107, https://doi.org/10.1029/2001JC000970, C8.
Shibayama, T., Saito, E., Okayasu, A., 1991. Effect of long waves to local sediment transport rate. In: Proc. of Coastal Sediments. pp. 129–138.
Shimozono, T., Tajima, Y., Kennedy, A., Nobuoka, H., Sasaki, J., Sato, S., 2015. Combined infragravity wave and sea-swell runup over fringing reefs by super typhoon haiyan. J. Geophys. Res. C: Oceans https://doi.org/10.1002/2015JC010760.
Sinnett, G., Feddersen, F., 2014. The surf zone heat budget: the effect of wave heating. Geophys. Res. Lett. 41, 7217–7226. https://doi.org/10.1002/2014GL061398.
Smit, P.B., Janssen, T., Holthuijsen, L., Smith, J., 2014. Non-hydrostatic modeling of surf zone wave dynamics. Coast. Eng. 83, 36–48.
Smith, G., Mocke, G.P., 2002. Interaction between breaking/broken waves and infragravity-scale phenomena to control sediment suspension transport in the surf zone. Mar. Geol. 187, 329–345.
Smithers, S., Hoeke, R., 2014. Geomorphological impacts of high-latitude storm waves on low-latitude reef islands - observations of the december 2008 event on Nukutoa, Takuu, Papua New Guinea. Geomorphology 222, 106–121. https://doi.org/10.1016/j.geomorph.2014.03.042.
Sous, D., Lambert, A., Rey, V., Michallet, H., 2013. Swash-groundwater dynamics in a sandy beach laboratory experiment. Coast. Eng. 80, 122–136.
Sous, D., Petitjean, L., Bouchette, F., Rey, V., Meulé, S., Sabatier, F., Martins, K., 2016. Field evidence of swash groundwater circulation in the microtidal rousty beach, france. Adv. Water Resour. 97, 144–155.
Steenhauer, K., Pokrajac, D., O'Donoghue, T., Kikkert, G., 2011. Subsurface processes generated by bore-driven swash on coarse-grained beaches. J. Geophys. Res. Oceans (1978-2012) 116.
Stockdon, H.F., Holman, R.A., Howd, P.A., Sallenger Jr, A.H., 2006. Emperical parameterization of setup, swash and runup. Coast. Eng. 53, 573–588.
Stokes, G.G., 1846. Report on recent researches in hydrodynamics. Brit. Ass. Rep 1, 1–20.
Suhayda, J.N., 1974. Standing waves on beaches. J. Geophys. Res. 79, 3065–3071. https://doi.org/10.1029/JC079i021p03065.
Sunamura, T., 1992. Geomorphology of Rocky Coasts. Wiley, Chichester.
Symonds, G., Huntley, D., Bowen, A.J., 1982. Two-dimensional surf beat: long wave generation by a time-varying breakpoint. J. Geophys. Res. 87, 492–498.
Symonds, G., Ranasinghe, R., 2000. On the formation of rip currents on a plane beach. In: Proc. of 29th Int. Conf. on Coast. Eng. ASCE, New York, pp. 468–481.
Talbot, M.M.B., Bate, G.C., 1987. Rip current characteristics and their role in the exchange of water and surf diatoms between the surf zone and nearshore. Estuar. Coast. Shelf Sci. 25, 707–720.
Tanimoto, T., 2005. The oceanic excitation hypothesis for the continuous oscillations of the earth. Geophys. J. Int. 160, 276–288. https://doi.org/10.1111/j.1365-246X.2004.02484.x.
Tatavarti, V.S.N., Huntley, D.A., Bowen, A.J., 1988. Incoming and outgoing wave interactions on beaches. In: ASCE, N.Y. (Ed.), International Conference on Coastal Engineering. 21.
Thomson, J., Elgar, S., Raubenheimer, B., Herbers, T.H.C., Guza, R.T., 2006. Tidal modulation of infragravity waves via nonlinear energy losses in the surfzone. Geophys. Res. Lett. 33, https://doi.org/10.1029/2005GL025514, L05601.
Thornton, E.B., MacMahan, J.H., Sallenger Jr, A.H., 2007. Rip currents, mega-cusps, and eroding dunes. Mar. Geol. 240, 151–167.
Tissier, M., Bonneton, P., Michallet, H., Ruessink, B.G., 2015. Infragravity-wave modulation of short-wave celerity in the surf zone. J. Geophys. Res. Oceans 120, 6799–6814. https://doi.org/10.1002/2015JC010708.
Tissier, M., Bonneton, P., Ruessink, B., 2017. Infragravity waves and bore merging. In: Proceedings of the Conference Coastal Dynamics 2017. ASCE, Helsingør, Denmark, pp. 451–460.
Traer, J., Gerstoft, P., 2014. A unified theory of microseisms and hum. J. Geophys. Res. 119, https://doi.org/10.1002/2013JB010504.
Tucker, M., 1950. Surfbeats: sea waves of 1 to 5 minutes period. In: Proc. R.Soc. London A 202-565-573.
Turner, I.L., 1998. Monitoring groundwater dynamics in the littoral zone at seasonal, storm, tide and swash frequencies. Coast. Eng. 35, 1–16.
Turner, I.L., Coates, B.P., Acworth, R.I., 1997. Tides, waves and the super-elevation of groundwater at the coast. J. Coast. Res. 46–60.
Turner, I.L., GC, R., MJ, A., MS, A., 2015. Groundwater fluxes and flow paths within coastal barriers: observations from a large-scale laboratory experiment (BARDEX II). Coast. Eng. https://doi.org/10.1016/j.coastaleng.2015.08.004.
Turner, I.L., Masselink, G., 1998. Swash infiltration-exfiltration and sediment transport. J. Geophys. Res. Oceans (1978-2012) 103, 30813–30824.
Turner, I.L., Masselink, G., 2012. Coastal gravel barrier hydrology-observations from a prototype-scale laboratory experiment (BARDEX). Coast. Eng. 63, 13–22.
Turner, I.L., Nielsen, P., 1997. Rapid water table fluctuations within the beach face: implications for swash zone sediment mobility?. Coast. Eng. 32, 45–59.
Uchiyama, Y., McWilliams, J.C., 2008. Infragravity waves in the deep ocean: generation, propagation, and seismic hum excitation. J. Geophys. Res. 113, C07029. https://doi.org/10.1029/2007JC004562.
Van Dongeren, A., Bakkenes, H.J., Janssen, T., 2002. Generation of long waves by short wave groups. Coast. Eng. 10.
Van Dongeren, A., Battjes, J., Janssen, T., van Noorloos, J., Steenhauer, K., Steenbergen, G., Reniers, A., 2007. Shoaling and shoreline dissipation of low-frequency waves. J. Geophys. Res. 112, https://doi.org/10.1029/2006JC003701, C02011.
Van Dongeren, A.R., Lowe, R., Pomeroy, A., Trang, D., Roelvink, D., Symonds, G., Ranasinghe, R., 2013. Numerical modeling of low-frequency wave dynamics over a fringing coral reef. Coast. Eng. 73, 178–190.
Van Dongeren, A.R., Reniers, A.J.H.M., Battjes, J.A., Svendsen, I.A., 2003. Numerical modeling of infragravity wave response during Delilah. J. Geophys. Res. 108, 3288. https://doi.org/10.1029/2002JC001332.
Van Rijn, L., 2009. Prediction of dune erosion due to storms. Coast. Eng. 56, 441–457.
Vetter, O., Becker, J., Merrifield, M., Pequignet, A., Aucan, J., Boc, S., Pollock, C., 2010. Wave setup over a Pacific island fringing reef. J. Geophys. Res. Oceans 115, 1–13. https://doi.org/10.1029/2010JC006455.
Vilibić, I., Monserrat, S., Rabinovich, A., Mihanović, H., 2008. Numerical modelling of the destructive meteotsunami of 15 June, 2006 on the coast of the Balearic islands. Pure Appl. Geophys. 165, 2169–2195. https://doi.org/10.1007/s00024-008-0426-5.
Vousdoukas, M.I., Wziatek, D., Almeida, L.P., 2012. Coastal vulnerability assessment based on video wave run-up observations at a mesotidal, steep-sloped beach. Ocean Dyn. 62, 123–137. https://doi.org/10.1007/s10236-011-0480-x.
Thiel de Vries, J. S. M., Van, 2009. Dune erosion during storm surges. Phd. Delft University of Technology.
de Vries, S., Hill, D., de Schipper, M., Stive, M., 2011. Remote sensing of surf zone waves using stereo imaging. Coast. Eng. 58, 239–250. https://doi.org/10.1016/j.coastaleng.2010.10.004.
Wargula, A., Raubenheimer, B., Elgar, S., 2014. Wave-driven along-channel subtidal flows in a well-mixed ocean inlet. J. Geophys. Res. Oceans 119, 2987–3001. https://doi.org/10.1002/2014JC009839.
Webb, S., Zhang, X., Crawford, W., 1991. Infragravity waves in the deep ocean. J. Geophys. Res. 96, 2723–2736.
Webb, S.C., 2007. The earth's 'hum' is driven by ocean waves over the continental shelves. Nature 445, 754–756. https://doi.org/10.1038/nature05536.
Webb, S.C., 2008. The earth's 'hum': the excitation of Earth normal modes by ocean waves. Geophys. J. Int. 174, 542–566. https://doi.org/10.1111/j.1365-246X.2008.03801.x.
Whitham, G.B., 1974. Linear and Nonlinear Waves. John Wiley & Sons.
Williams, M.E., Stacey, M.T., 2016. Tidally discontinuous ocean forcing in bar-built estuaries: the interaction of tides, infragravity motions, and frictional control. J. Geophys. Res. 121, 571–585. https://doi.org/10.1002/2015JC011166.
Wright, L.D., Short, A.D., 1984. Morphodynamic variability of surf zones and beaches: a synthesis. Mar. Geol. 56, 93–118.
Young, A.P., Guza, R.T., O'Reilly, W.C., Burvingt, O., Flick, R.E., 2016. Observations of coastal cliff base waves, sand levels, and cliff top shaking. Earth Surf. Process. Landf. 41, 1564–1573. https://doi.org/10.1002/esp.3928.
Young, I.R., 1989. Wave transformation over coral reefs. J. Geophys. Res. Oceans 94, 9779–9789. https://doi.org/10.1029/JC094iC07p09779.
Zabotin, N.A., Godin, O.A., Bullett, T.W., 2016. Oceans as a major source of waves in the thermosphere. J. Geophys. Res. Space Phys. 121, 3452–3463. https://doi.org/10.1002/2016JA022357.
Zijlema, M., Stelling, G., Smit, P., 2011. SWASH: an operational public domain code for simulating wave fields and rapidly varied flows in coastal waters. Coast. Eng. 58, 992–1012.